Summer 2021

Development of a Pneumatically Controllable Microdroplet Generator with Electrical Sensing

Gnanesh Nagesh
University of Windsor

Development of a Pneumatically Controllable Microdroplet Generator with Electrical Sensing

By

Gnanesh Nagesh

A Thesis

Submitted to the Faculty of Graduate Studies

through the Department of Mechanical, Automotive and Materials Engineering

in Partial Fulfillment of the Requirements for

the Degree of Master of Applied Science at the

University of Windsor

Windsor, Ontario, Canada

Development of a Pneumatically Controllable Microdroplet Generator with Electrical Sensing

By

Gnanesh Nagesh

APPROVED BY:

_____

B. Balasingam
Department of Electrical & Computer Engineering

_____

O. A. Jianu
Department of Mechanical, Automotive & Materials Engineering

_____

D. Ting, Co-Advisor
Department of Mechanical, Automotive & Materials Engineering

_____

J. Ahamed, Co-Advisor
Department of Mechanical, Automotive & Materials Engineering

April 26, 2021

DECLARATION OF CO-AUTHORSHIP/PREVIOUS PUBLICATION

I. Co-Authorship

I hereby declare that this thesis incorporates material that is result of joint research of the author, his supervisors Prof. David S-K Ting and Prof. Mohammed Jalal Ahamed, and Hualong Wang. In all cases, the key ideas, primary contributions, experimental designs, data analysis, interpretation, and writing were performed by the author. The contribution of the professors included providing feedback on refinement of ideas and editing of the manuscript. The contribution of co-author Hualong Wang was primarily towards the expertise in experimental which has been instrumental for the research presented in chapter 2.

I am aware of the University of Windsor Senate Policy on Authorship and I certify that I have properly acknowledged the contribution of other researchers to my thesis and have obtained written permission from each of the co-author(s) to include the above material(s) in my thesis.

I certify that, with the above qualification, this thesis, and the research to which it refers, is the product of my own work.

II. Previous Publication

This thesis includes 2 original paper that has been previously published/submitted for publication in peer reviewed journal, as follows:

Thesis Chapter	Publication	Publication Status
Chapter 2	G. Nagesh, H. Wang, D. S.-K. Ting, and M. J. Ahamed, "Development of a rapid manufacturable microdroplet generator with pneumatic control," Microsyst. Technol., Oct. 2020, "https://dx.doi.org/10.1007/s00542-020-05052-9"	Journal (Published)
Chapter 3	G. Nagesh, D. S.-K. Ting, and M. J. Ahamed, "Capacitive detection and characterizing of droplets in a T-junction-based droplet generator".	Submitted to Sensors and Actuators A: Physical (Under Review)

I certify that I have obtained a written permission from the copyright owners to include the above published material in my thesis. I certify that the above material describes work completed during my registration as a graduate student at the University of Windsor.

III. General

I declare that, to the best of my knowledge, my thesis does not infringe upon anyone's copyright nor violate any proprietary rights and that any ideas, techniques, quotations, or any other material from the work of other people included in my thesis, published or otherwise, are fully acknowledged in accordance with the standard referencing practices. Furthermore, to the extent that I have included copyrighted material that surpasses the bounds of fair dealing within the meaning of the Canada Copyright Act, I certify that I have obtained a written permission from the copyright owners to include such material in my thesis.

I declare that this is a true copy of my thesis, including any final revisions, as approved by my thesis committee and the Graduate Studies office, and that this thesis has not been submitted for a higher degree to any other University or Institution.

ABSTRACT

Microfluidic droplet generation is popular in lab-on-a-chip based biochemical analysis because it can provide precise and high throughput fluids in the form of small droplets. This thesis presents a T-junction microdroplet generator with pneumatic actuation for regulating droplet size and a capacitance-based sensor with real-time sensing capability for characterizing droplet composition and size. The multi-layer device developed in this thesis is compatible with rapid manufacturing using a desktop-based laser cutter to fabricate the fluidic and pneumatic layers. A finite element based numerical model was developed to predict the best operating and geometric parameters for droplet generation. It was revealed that the model could generate monodisperse droplets with a capillary number of 0.0007 for an aspect ratio of 1.11:1 and that the electrode width to droplet size ratio of 1:0.95 was the best size for sensing droplet movement. The results with pneumatic control showed working pneumatic pressure of up to 0.4 MPa is achievable, resulting in a 38% reduction in droplet size compared to a reference droplet. The continuous fluid used in the model was 0.1 ml/min, whereas the conventional method was 0.19 ml/min, resulting in a 38 percent reduction in droplet size. The droplet size decreased by 9.7 percent as the pressure inside the pneumatic chamber is increased by 0.1 MPa. As a result of this reduction, the capacitance value sensed decreases by 4.7 percent when a droplet (dispersed material) is fully positioned between electrodes, whereas it increases by 2.0 percent when only continuous fluid is present. Similarly, in material characterization, when the dispersed material was changed, the variation in capacitance for a droplet movement was observed to change. The multi-layer droplet generation, with simple and simultaneous sensing as well as regulation capability presented in this thesis, can be useful for the development of precision droplet generators with closed-loop control.

DEDICATION

To my family, for their continuous support.

ACKNOWLEDGEMENTS

I would like to express my gratitude to Dr. Jalal Ahamed, my thesis advisor at the University of Windsor, for his unwavering support, encouragement, and guidance over the past two years. He consistently encouraged me to learn and develop at my rate, making this an inspiring experience.

I would also like to thank Dr. David Ting, my thesis co-advisor, for his expertise, feedback, and encouragement during my research, which has allowed me to develop and bring out the best in me every time.

CMC Microsystems, for supporting me with this work, and providing me the necessary equipment and devices on time so I can complete the experimental portion of this research.

Thank you to my committee members Dr. Balakumar Balasingam and Dr. Ofelia A. Jianu, for taking the time to review my thesis and provide feedback throughout my research.

My research team at the MicroNano laboratory for their input and suggestions. This was a team effort that I was happy to be a part of.

TABLE OF CONTENTS

LIST OF TABLES

LIST OF FIGURES

NOMENCLATURE

ρ	Density of the fluid, kg/m^3
u	Flow speed, m/s
L	Characteristic linear dimension, m
μ	Dynamic viscosity of the fluid, Pa-s
γ	Interfacial tension, N/m
β	Coefficient of thermal expansion, K^{-1}
ΔT	Temperature difference between the surface and the bulk of the fluid, K
$\Delta\rho$	Density difference between the two immiscible fluids, kg/m^3
g	Acceleration due to gravity, m/s^2

CHAPTER 1

INTRODUCTION

The field of microfluidics deals with micro-scale flows and it began to develop 40 years ago with the introduction of microfluidics-based nozzles for ink jet printers for generating small-scale droplets using silicon as the substrate material [1]. Following that, numerous developments were made in microfluidics including a focus to interface different physics into a small chip, for example, fluid-structure interaction for droplet actuation or electrodes for droplet sensing. Fluid-structure interaction is especially important to achieve actuation or fluid displacement, for example, to create a micro pumping or microdroplet dispenser. Apart from fluid displacing, around 1990, the first integrated microfluidic structure for chemical analysis was designed [2]. Along with actuation and sensing, it motivated the development of various application-oriented demonstrations including achieving on-chip biochemical analysis termed as ‘lab-on-a-chip’. Around that time, microfluidics, also known as lab-on-a-chip or micro total analysis (μTAS), became well-known [3]. Microfluidic systems became popular in biochemical analysis because of their ability to operate and manipulate fluids at the micro-scale, which contributed to the model's low cost, low manufacturing material usage, short analysis time, and low reagent use. One of the most fundamental functions of microfluidic systems is the generation of emulsions using microfluidic devices designed to supply customized emulsions in material synthesis, which has given rise to some of its applications. Which is widely termed a microfluidic droplet generator where it uses immiscible liquids in microfluidic channel networks to create uniform-sized liquid-liquid droplets. The ability of the droplet generator to reproduce a precise number of droplets, control the size of the droplets generated, and generate droplets in a short amount of time made it

a desirable system. These generated droplets have been used to create reagents for chemical reactions and other applications that involve a precise number of repeated volumes of reagents.

Microfluidic droplet generator systems are capable of controlling and regulating fluids in the range of microlitre to picolitre, and the scale of these systems is often within the range of few micrometers to a nanometer. Micro droplet generators are used in many biochemical applications, including drug delivery [4], [5], DNA structure analysis [6], biomolecule synthesis [7], microreactors [8], and diagnostics [9]. Protein crystallization is an example of a similar application in which proteins are crystallized not only to understand structural details but also to help understand the functions and mechanisms involved in a variety of physiological processes. Protein crystallization occurs when the soluble protein concentration in a mixture exceeds the precipitant concentration, resulting in high-quality protein crystals. This process is affected by temperature, pH, additives, and other factors. As a result, many trials must be carried out to determine the best parameter values for protein crystallization [10]. The microfluidic droplet generator is used in protein crystallization because of its high throughput generation and low reagent consumption. Where the protein crystallization is achieved using monodisperse droplets comprising a protein-precipitant fluid mixture. The four types of protein crystallization methods available are vapor diffusion, microbatch, microdialysis, and free-interface diffusion and among these the first two types are considered in microfluidic droplet generation [11].

In the microbatch process, a T-junction design is used, in which a dispersed fluid has three inlets containing the protein, precipitant, and buffer solutions. Which are mixed at the T-junction interface, and droplets are generated using the mixed solution. Since the aim is to find the best parameter values for protein crystallization, many trial droplets are generated by varying the soluble concentration, making each droplet unique. This is done by varying the fluid flow speeds,

which changes the concentration of these liquids in the formed droplets. The droplets are then moved to a capillary channel for incubation, where the protein's crystallization is analysed using X-ray diffraction to determine the best parameter value to consider for crystallization. In the vapor diffusion process, two separate dispersed fluids are used to generate alternate droplets in the micro channel. One of the alternative droplets contained a protein and precipitant mixture, while the other involved a high concentration of NaCl solution. The water in the generated protein-precipitant droplet begins to diffuse into the NaCl droplets, increasing the crystallization process by increasing the protein concentration. This diffusion continues until the osmotic pressure balance between the two droplets is achieved. Like earlier the crystallized protein is analysed to understand the optimum value. In both approaches, the flow rate is changed to generate different droplet concentrations that are then analysed to find the best parameter values.

Similarly, in the analysis of drug dose-response, a differential flow rate is used to produce various concentrations of drugs in droplets. The biological effects generated by a chemical compound of a drug are closely related to its concentration. As a result, various concentrations of drug droplets are generated and analysed for their effects, and they are varied based on differential flow rate or Taylor-Aris dispersion phenomenon [12]. In these applications, droplet generation combined with fluid regulation, detection, and characterization is sought after. Droplets are generated and controlled by a variety of microfluidic devices, so designs that can generate a precise and controllable number of droplets are in high demand.

Generally, droplet generators that offer precise control over droplet size are developed using semiconductor-based fabrication involving photolithography, dry/wet chemical etch, and bonding, which requires specialized microfabrication equipment and techniques [13]–[16]. These fabrication processes are favored, as they ensure a high degree of feature accuracy, allowing highly

precise and repeatable droplet generation. It is often expensive, however, and it has a long development time from design to device realization. To reduce fabrication cost and production time, there are various simple and cost-effective alternative fabrication methods, such as 3D printing [17], liquid molding [18], rapid manufacturing [19]–[21], and laser cutters/engravers. These have great success in terms of both reducing cost and manufacturing small micro/nanoscale features. 3D-printed and rapid manufacturable microfluidic droplet generators have received a lot of attention in recent demonstrations of their precision over droplet size, quick production time, low-cost manufacturing, and control of droplet volume [22], [23]. They have propelled the development of many different types of droplet generator designs that are compatible with both semiconductor-based fabrication and rapid manufacturing.

Among different droplet generator designs, T-junction [24]–[28], flow-focusing [29]–[34], and co-flow [35]–[38] are the three most common. The T-junction design has been widely used due to its simplicity.

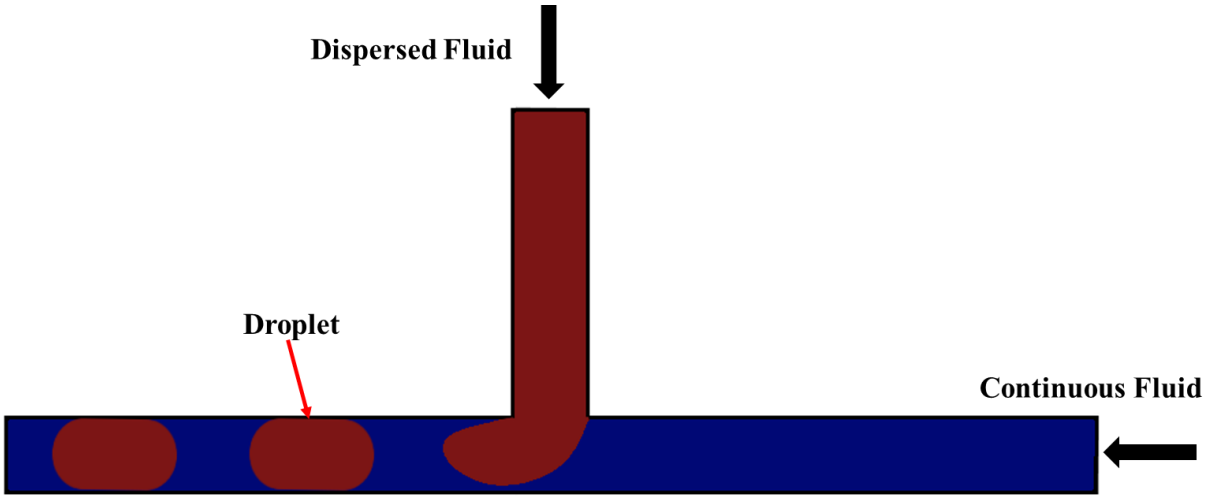

Figure 1-1: Schematic illustration of a classical T-junction droplet generator.

In a classical T-junction design, the droplet generators use oil and an immiscible aqueous fluid, so that they do not mix downstream. The oil droplet can be created in aqueous fluid or aqueous droplets in the oil fluid [39]. The fluid used to make droplets is generally referred to as dispersed fluid and the one that splits the fluid flow to produce droplets is a continuous fluid as shown in Figure 1-1. The dispersed fluid flows and changes direction at the interface in a T-junction design. Necking occurs because of interfacial tension and differential pressure, and the droplets gradually separate from their parent fluid and flow with the continuous fluid.

LITERATURE REVIEW

To study and understand the design, controls, and sensing aspects of T-junction-based droplet generation in microfluidics, the available literature on manufacturing processes, droplet regulation, and droplet quantification and characterization are considered. As a result, some of the research papers on these factors focused on microdroplet generators to see how they function are looked at.

Photolithography is the most common manufacturing process in micro/nano electromechanical systems (MEMS/NEMS), and it is also used to develop models in microfluidics. Shen et al [40] used a microfluidic droplet generator with a T-junction configuration to produce a precise number of droplets with an integrated optical sensor to distinguish and quantify the generated droplets at the output. The model was developed using the soft lithography process, which involves two steps: first, forming a mold using photolithography, and then pouring a soft polymer called Polydimethylsiloxane (PDMS) into the mold to create a fluidic layer, where the pattern formed in the mold is transferred to the PDMS fluidic layer. So, in detail the first step is to make the mold, which involves spin-coating a 128 μm thick layer of negative photoresist on top of a 3-inch silicon

wafer. The required pattern is then designed using any CAD (computer-aided design) tool and transferred to a transparent photomask, which will be later used to transfer the pattern onto the photoresist using photolithography process using UV light. After UV exposure, the photoresist becomes insoluble after being exposed to UV light; the soluble photoresist is removed, and the insoluble is retained as a pattern guide on the wafer. The wafer is then developed for 10 minutes before being rinsed with IPA (Isopropyl Alcohol). Finally, a mold is created and a nanoscale coating of chromium copper is sputtered on it to enable the easy removal of the PDMS layer. So, a 4 mm layer of PDMS is poured on top of the mold to transfer the pattern from the mold to the PDMS layer. To remove all the bubbles, this PDMS layer with mold was kept in a vacuum for 45 minutes. After that, it was kept in the oven for 2 hours at 60 ºC to have it set before being peeled off. The peeled-off layer is then bonded to a flat PDMS layer using oxygen plasma treatment to seal off the fluidic layer. The model is then kept in an oven for 2 h at 80 ºC to ensure the bonding effect. The surface properties of PDMS change from hydrophobic to hydrophilic because of this treatment, resulting in an unstable droplet generation. To prevent this, the model is left overnight to restore the hydrophobic properties of the surface. After the manufacturing process, the developed model is attached to inlets and outlets. Yang et al [41] used a flow-focusing design integrated with a series of T-junction designs to generate sub-femtolitre droplets as seen in Figure 1-2 .They used soft lithography with PDMS (soft polymer) as their fluidic layer and photolithography as their manufacturing method for mold manufacturing, like previous paper. A 30 µm thick photoresist is used to transfer the pattern onto a silicon wafer. So, the created mold is used where a 5 mm thick PDMS layer is poured onto it and waited till all the bubbles disappeared. Once it did the layer is cured in an oven at 70 ºC for 3 h. The layer is then peeled away from the mold, and the inlets and outlets are drilled out with a metal pipe. The fluidic layer is then bonded

to a glass slide after 1 minute of exposure to oxygen plasma. The model is then kept at 120 ºC overnight to restore its hydrophobicity.

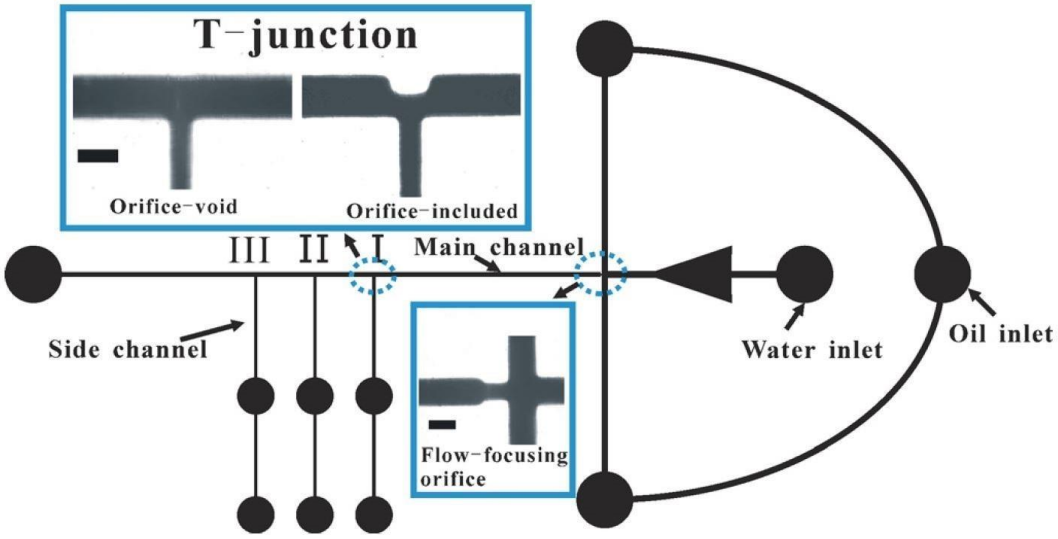

Figure 1-2: Schematic of a previous experimental microfluidic chip where they used flow-focusing and T-junction to create sub-femtolitre droplets [41].

The differential flow rate between the continuous and dispersed fluids is the most generally used as a droplet regulation method in T-junction-based generators. In this control method, the flow rate of the dispersed fluid is kept constant while the flow rate of the continuous fluid is varied, or both fluid flow rates are varied simultaneously to generate droplets of various sizes. For their model, Donvito et al [19] used a T-junction design, which was developed using a 3D printing technique. They wanted to see if there was a correlation between the length of a droplet and the ratio of continuous to dispersed fluid flow rates. So, they varied the flow rate of dispersed fluid from 1-35 µl/min and continuous fluid from 8-45 µl/min for a series of 6000 samples and discovered $L / w_c = 1 + \alpha Qd / Qc$. Where L is the droplet length, w_c is the width of continuous fluid, Qd is the flow rate of dispersed, α is the constant which depends on the T-junction geometry, and Qc is the flow rate of a fluid. Figure 1-3 depicts the relationship between droplet length and flow rate ratio. They

were able to regulate the droplet length between 155 to 52 µm using this differential flow rate. Yeh et al [42] created a series of four flow-focusing designs which were connected to four individual dispersed fluid inlets. These dispersed fluids being created using three micro mixers with two inlets, one with a 70% concentration of trypan blue solution and the other with only deionized water (0% concentration trypan blue solution). The micromixer was used to make four separate concentrations of trypan blue solution: 70, 43, 21, and 0% for dispersed fluid. Then, for four flow-focusing designs, these four solutions were used as dispersed fluids and sunflower seed oil as continuous fluids. So, the flow-focusing design was able to generate four different concentration droplets simultaneously. The droplets were then regulated in three trials using differential flow rate, where they kept dispersed fluid flow rate constant at 2.0, 2.5, and 3.0 µl/min while increasing the continuous flow rate from 4 to 12 µl/min, as shown in Figure 1-4. They were able to regulate the droplet size between 60 and 105 µm because of this.

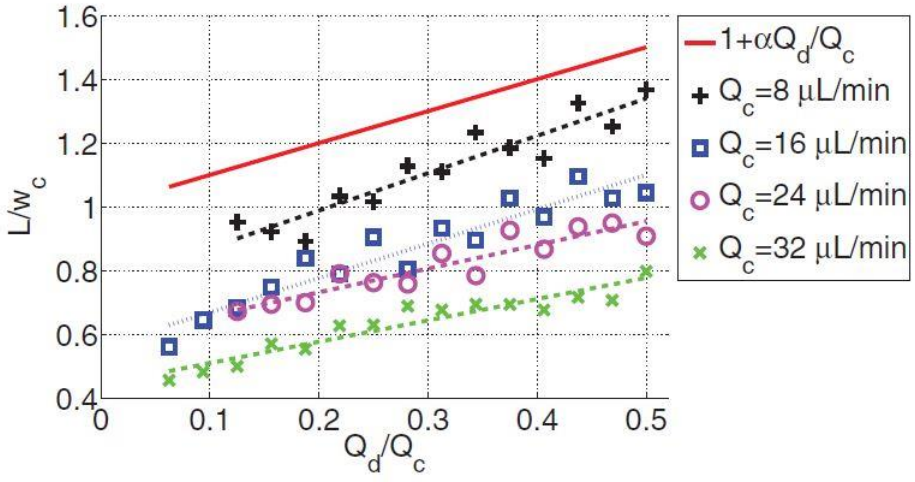

Figure 1-3: An analysis showing the comparison droplet length between flow rate ratio with α = 1 [19].

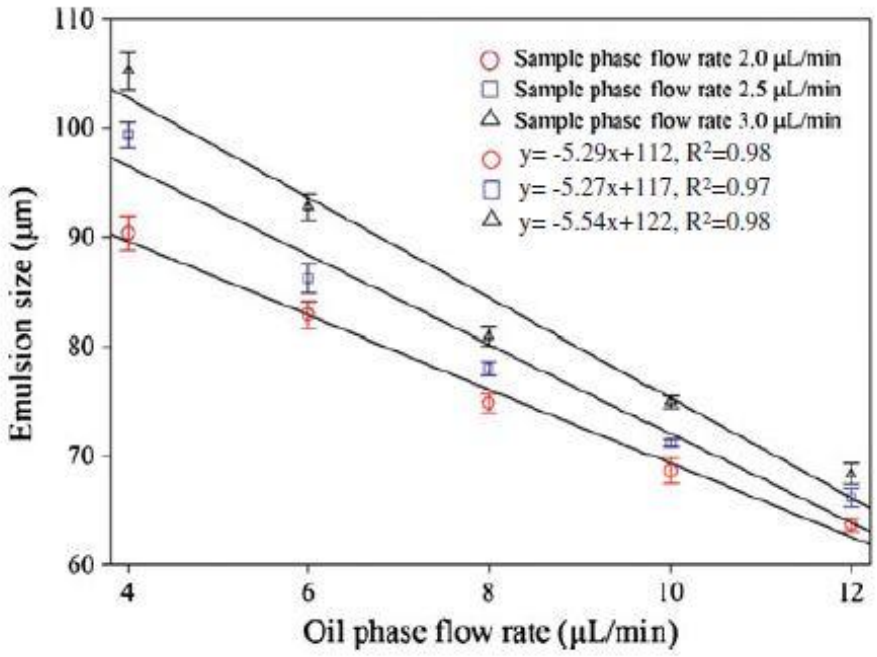

Figure 1-4: The relationship between generated droplet size with different continuous fluid flow rates [42].

The quantification of generated droplets is essential after droplet generation. So, by detecting, this thesis will be able to quantify the droplet's various important parameters including composition, speed, and size distribution. The most widely used droplet quantification approach is the optical method, which employs a light sensor to distinguish between dispersed and continuous fluids based on their refractive index. Shivhare et al [43] have developed an optofluidic system for in-situ measurement of droplet quantification and droplet mean size. They used a flow-focusing design with two groves etched near the output channel, one for an optical fiber to produce a focused illumination beam and the other for a photodiode, with both grooves filled with index-matching liquid to minimize reflection losses, as shown in Figure 1-5. They used a non-hazardous laser source in the range of 1550 nm in this experiment. The optical detection system is made up of two parts: illumination and data collection. For illumination, a voltage regulator is used to obtain

a regulated voltage of ± 5V, which is then connected to a single-mode fiber-coupled to a laser diode for illumination. Multimode fiber coupled InGaAs photodiode was used to collect the scattered signal from the illuminator. This signal is amplified with a trans-impedance amplifier before being converted to digital by a microcontroller. The data is then analysed on a computer using Python code. When a droplet moves between the detection region and the laser beam, it obstructs the beam's passage, causing a pulse to be generated in the detected signal. They were able to detect and measure the mean droplet size using this principle. Gu et al [44] have used a flow-focusing design to generate the droplets with different concentrations. The detection of droplets is based on the idea that when a droplet reacts with a micro electrode inserted into a microfluidic channel, a chemical reaction occurs, resulting in a generation of charge which gets picked up by the electrodes. Here the microelectrode used is an Ag/AgCl microelectrode and Platinum black (Pt-black) microelectrode. Electrodepositing platinum nanoparticles on a bare platinum microelectrode produces the Pt-black microelectrode. This results in a flower-like microstructure, which increases the electrocatalytic behavior of hydrogen peroxide (H_2O_2) oxidation. As shown in Figure 1-6, two microelectrodes are inserted at the fluidic line's output to sense the droplets. As a droplet encounters these two microelectrodes, two reactions occur one where β-D-glucose reacts with oxygen to form D-gluconic acid and Hydrogen peroxide, and the other where the generated Hydrogen peroxide reacts with Ag/Agcl microelectrode to form oxygen and hydrogen by releasing two electrons. So, due to the chemical reaction, an electric charge is generated when a droplet encounters two electrodes. Using this they were able to detect the number of droplets generated and even the concentration of D-gluconic acid in the generated droplet with the amplitude of the generated current.

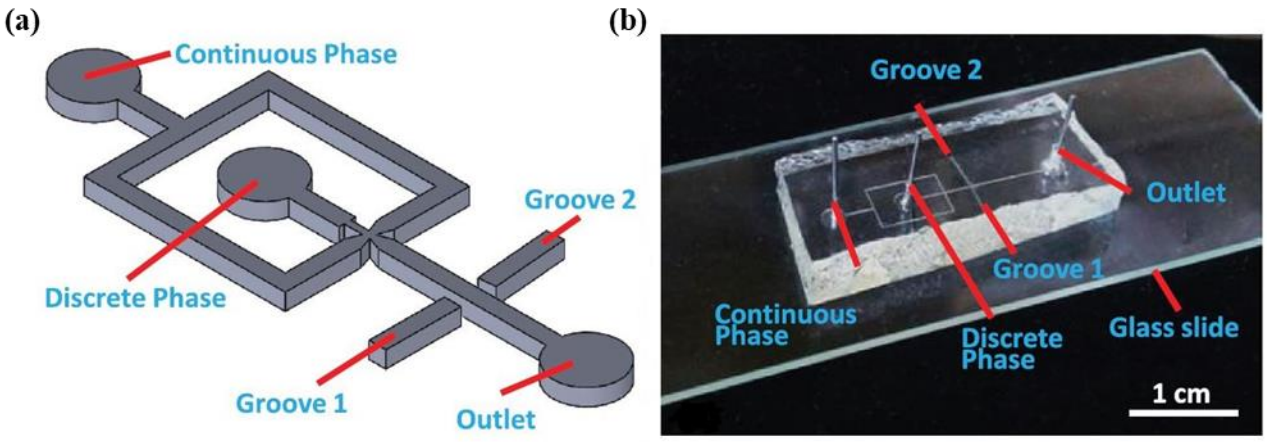

Figure 1-5: The droplet generator with an optofluidic system for an in-situ measurement,(a) schematic design of the device, and (b) The fabricated and assembled model [43].

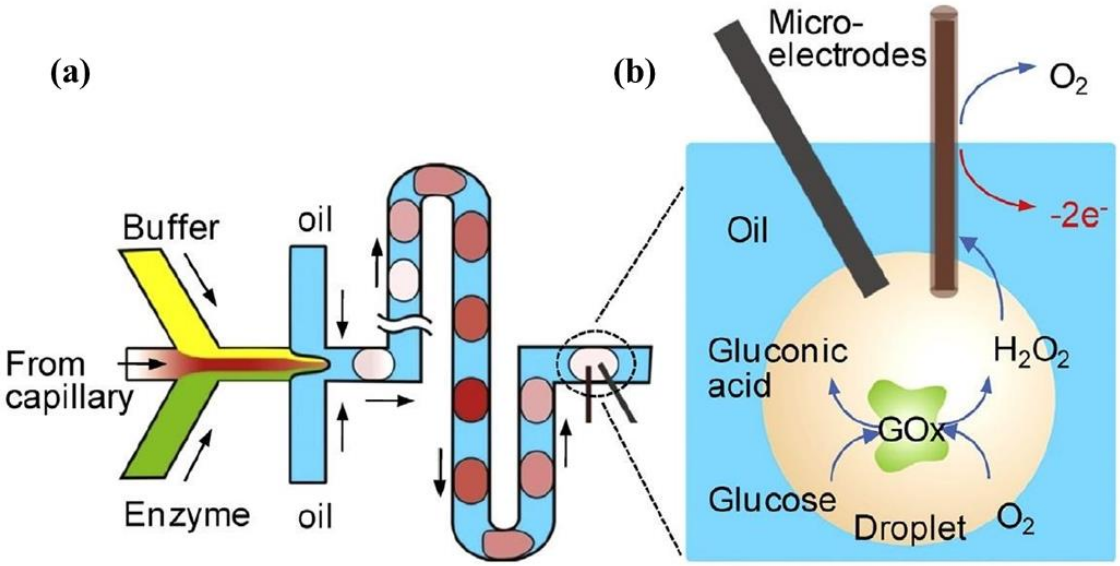

Figure 1-6: An electrochemical sensor is used for detection of droplets, (a) schematic of microfluidic droplet generator, and (b) electrochemical reaction during the detection of glucose in a droplet [44].

The following studies have been carried out from previous research:

1. The traditional approach for regulating droplets is to create a differential flow rate, in which the dispersed fluid flow rate is kept constant while the continuous fluid flow rate is increased to reduce droplet size.
2. The optical method is widely used for quantification and characterization, where the differential refractive index is used to differentiate the fluids so that the generated droplets can be quantified. In electrochemistry, the chemical reaction at the electrode surface as it encounters droplets generates an electrical charge, which is then used to quantify the droplets.
3. For manufacturing the droplet generator mostly various soft lithography-based methods are used involving replica molding. The master for replica mold is created using photolithography, and the pattern from the mold is then transferred to the soft polymer material to develop the model.

This study aims to develop a different approach to controlling droplet size that focuses on regulating droplets without increasing continuous fluid consumption while minimizing droplet size. The traditional approach, which uses a differential flow-based control system, is not fast and requires multiple pumping and complexity in controlling the pumps. The focus is to develop a simpler but accurate droplet sensing based on the electrical method. The conventional optical method requires an external camera or complicated optical sensors. The use of additional equipment and the integration of sensors in the quantification and characterization of droplets is a bit complicated during the manufacturing process, so a simpler sensor is needed.

In two-phase flow, inertia, viscous shear, interfacial tension, and buoyancy are the most significant forces to consider. The Reynolds number, which is the ratio of inertia to viscosity, the capillary number, which is the ratio of viscous to interfacial, the Grashof number, which is the ratio of buoyancy to viscous, the Bond number, which is the ratio of gravitational to interfacial, and the Weber number, which is the ratio of inertia to interfacial, are all used to describe these forces, as shown in Table 1 [45]–[47]. Since the models in microfluidics are in micro-scale, the flow rates are low, and the high surface-to-volume ratio makes inertia and gravity negligible in comparison to viscous and interfacial forces because of that the Grashof, Bond, and Weber are not considered. In the droplet generator, the capillary number plays a significant role in deciding the size of the generated droplet size.

Table 1: The dimensionless number that is considered during two-phase flow.

Dimensionless number	**Equation**	**Definition**
Reynolds number	$\frac{\rho u L}{\mu}$	Inertia/viscous
Capillary number	$\frac{\mu u}{\gamma}$	Viscous/interfacial
Grashof number	$\frac{L^3 \rho^2 \beta \Delta T}{\mu^2}$	Buoyancy/viscous
Bond number	$\frac{\Delta \rho g L^2}{\gamma}$	Gravitational/interfacial
Weber number	$\frac{\rho u^2 L}{\gamma}$	Inertia/interfacial

OBJECTIVES

Our objective is to focus on and improve the control mechanism and sense of the droplet generator. The first objective is to develop a new control mechanism that will improve droplet regulation. A differential flow rate is developed in a conventional droplet regulation method to reduce droplet size by increasing the continuous fluid flow rate, but this increases fluid consumption. So, this thesis try to regulate droplet size by implementing a pneumatic chamber on top of the T-junction where both fluid flow rates are kept constant. This chamber employs a flexible membrane, which decreases the size of the droplets at the junction without the use of additional continuous fluid.

The second objective is developing an electrical sensing mechanism that can be interfaced with the droplet generator. The integration of electrochemical-based electrodes or optical fibres in the quantification of droplets is complex during manufacturing, so to avoid this, this thesis is implementing a simple capacitive-based sensor for quantification and characterization of generated droplets. This thesis proposes integrating a copper foil as a capacitance electrode for the sensor during the assembly process at the fluidic line.

CHAPTER 2

DESIGN AND DEVELOPMENT OF A MICRODROPLET GENERATOR WITH PNEUMATIC CONTROL

A versatile microfluidic droplet generator can generate monodisperse droplets that can be regulated to the desired size. Droplet regulation for the desired size is a necessity in some applications, such as protein crystallization and drug dose-response studies, as previously mentioned. Protein crystallization parameters are optimized to find the optimal values for higher-quality protein crystals. These optimal parameter values are determined by generating many trial droplets and altering the concentration of soluble in each droplet to understand the effect of the parameters on crystallization. Similarly, in drug-response, many drug dose concentrations are generated as droplets to find the optimal value. As previously stated, the traditional approach employs a differential flow rate, and as the droplet size decreases, the amount of continuous fluid consumed increases proportionally. As a response, this research intend to minimize this by integrating a pneumatic chamber on top of the junction, where the flow rate of both fluids is maintained constant, but the droplet size is regulated by the pressure within the pneumatic chamber.

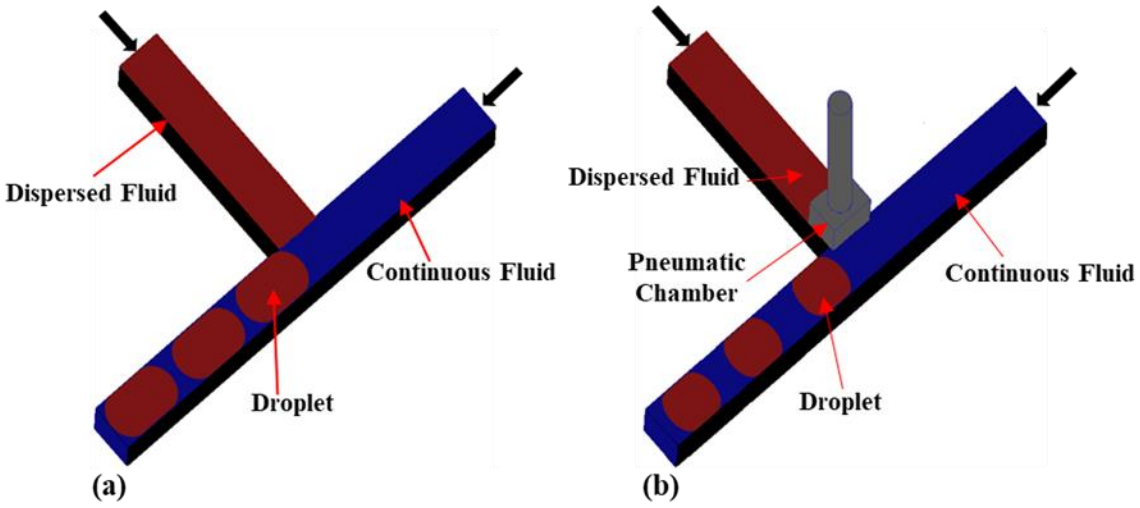

Figure 2-1: 3D schematic showing (a) classical T-junction droplet generator design, and (b) the conceptual design of the proposed droplet generator with pneumatic control. Droplets are generated at the junction and the pneumatic chamber located on top of the junction allows for additional control of droplet sizes.

Figure 2-1 (a) portrays the formation of droplets in a classical T-junction design. The dispersed fluid flows perpendicularly with respect to the continuous fluid until they meet at the T-junction. The dispersed fluid changes its direction at the interface, it starts to form into capture-shaped droplets, and the continuous fluid shears the droplet from the dispersed fluid. After the droplet is formed, it is conveyed by the continuous fluid flowing down the same channel. A versatile system would allow for accurate control and the precise generation of droplets of the desired size. Usually, the generated droplet size is controlled by the differential flow rate between fluids [40, 48], or by the addition of electrodes at defined spots, which, in turn, affects the flow rate of fluid [49], [50]. Controlling droplet size by manipulating flow alone requires secondary equipment, more space, and additional continuous fluid. In addition, automatic, precise, and small-scale control is challenging. Wu et al [51] have presented an interesting design with pneumatic pressure control to

regulate the droplet size using polydimethylsiloxane (PDMS) as a material and the photolithography process for fabrication, where the pneumatic chamber is constructed downstream of the junction were to control the droplets. The droplet size control was achieved by manipulating the local flow velocity and shear force by the pneumatic membrane placed downstream. Using this robust method, they were able to regulate the droplet size. In this chapter, the design by introducing a pneumatic pressure chamber on top of the junction is presented, as shown in Figure 2-1 (b), to regulate the droplet size. Since droplet size control using flow variation at the junction requires additional reagent to reduce the droplet size, it is often challenging to control precisely. In our design, in addition to fluid flow manipulated size control the research show additional droplet size controllability by regulating the dispersed fluid flow area due to the presence of pneumatic pressure inside the chamber. In this chapter, will present the design and development of the pneumatic control system.

This chapter presents a pneumatically controllable T-junction droplet generator that can vary the junction area vertically to control droplet size. The pneumatic pressure chamber placed on top of the junction provides additional control over droplets; this could be beneficial for further development of cost-effective microdroplet research and development. In the next section, will discuss the details of the numerical simulation of droplet generation. That will be followed by an outline of device structures and fabrication methods. Finally, will present prototype performance and characterization.

DEVICE DESIGN AND NUMERICAL ANALYSIS

To appreciate the various flow rates required for forming the desired droplets in the T-junction and to investigate the influence of geometric parameters (channel size, necking area, aspect ratio) a

numerical model is created to simulate the device performance. The numerical model tool assisted in understanding the influence of channel geometry, inlet flows, the interfacial tension between two immiscible fluids, and fluid contact angle on the droplet generation process. The numerical simulation was carried out using the commercial finite element model tool COMSOL 5.5. In this research the mesh was customized to reduce the computing time and keeping the accuracy of result by considering the finer elements in the preferred domains as can be seen in Figure 2-2. In comparison to the upstream channels of continuous fluid and dispersed fluid, the interface domain where the two immiscible fluids meet and the downstream channel where droplet movement is present has a finer mesh.

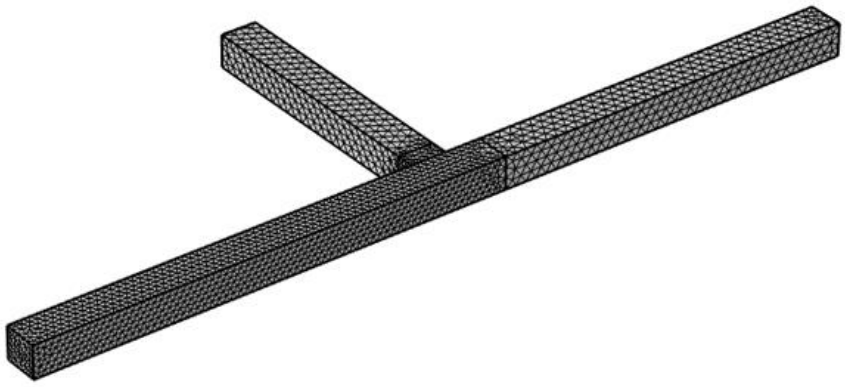

Figure 2-2: The meshing sizes considered during numerical simulation of droplet formation at T-junction flow channels.

This research invoked a multiphysics solver, the laminar two-phase flow, level-set physics, to solve for the fluid flow and the droplet formations. For resolving the involved fluid motion, the simulation called upon Navier-Stokes's equation and continuity equation:

$$\rho \frac{\partial u}{\partial t} + \rho(u \cdot \nabla)u = \nabla \cdot [-pI + \mu(\nabla u + (\nabla u)^T)] + F_{st} \quad (1)$$

$$\nabla \cdot u = 0 \quad (2)$$

where u is velocity (m/s), ρ is density (kg/m^3), μ is dynamic viscosity (Pa-s), p is pressure (Pa), I is the identity matrix, and F_{St} is a surface tension force (N/m^3). The droplet formation was simulated using a Level-set interface where the level set variable (Φ) was set, that is,

$$\frac{\partial \phi}{\partial t} + u \cdot \nabla \phi = \gamma \nabla \cdot \left(-\phi(1-\phi)\frac{\nabla \phi}{|\nabla \phi|} + \varepsilon \nabla \phi \right) \quad (3)$$

where Φ is the level set function, and γ and ε are numerical stabilization parameters. In the microfluidic droplet generator, the Reynolds number is typically less than 50 whereas our model is in the range of 0.4 therefore the laminar two-phase flow [52] inside the fluidic channels was solved together with a level set interface to trace the interface between the two immiscible fluids. The surface of the droplet is shown as a black outline around the droplet in Figure 2-3. For both continuous fluid and dispersed fluid, a level set function (Φ) is defined in simulation. Where the continuous fluid value would be Φ=1 and dispersed fluid Φ=0, as can be seen in the legend of Figure 2-3. The wetted wall with no slip [53], [54] boundary condition is imposed here, where the fluid contact angle and interfacial tension between two immiscible fluids play a major role in the simulated solution. Time-dependent with phase initialization is used to perform the calculation to understand the droplet formation over a period. The simulation was used to observe and analyze how the fluid velocity, individual surface tension, and geometry affect the droplet formation. The interfacial tension and viscous shear between the two immiscible fluids generally break up the droplet. As the dispersed fluid changes direction at the interface, the interfacial tension tries to decrease the surface area of the dispersed fluid, while the viscous shear force between the

continuous and dispersed fluid tries to increase it. Because of these two forces, a neck forms at the interface, where one is attempting to elongate and the other is attempting to minimize surface area. The neck thickness decreases as the fluid flows farther away from the interface, and eventually, a piece of fluid is broken from the fluid flow to form a droplet. This is the case when the droplet is in a dripping or tearing regime, but our model is simulated in a squeezing regime, so the droplet is created due to the pressure difference at the droplet's surface in the channel. When dispersed fluid enters a continuous channel, it blocks the flow, allowing pressure to build up on the rear side of the droplet, which is greater than the front side. As a result, the interfacial tension tries to minimize the surface area, while the differential pressure generated by the blockage of continuous fluid from the dispersed fluid tries to push it forward. As a result, the fluid begins to move from the higher to the lower pressure end. This causes the droplet to advance by rising the fluid's surface area in the continuous fluid line. As the interfacial stress attempts to reduce the surface area, necking begins to occur. The necking thins as the fluid goes forward until it reaches a point where it separates from its parent liquid and forms a droplet. For example, Figure 2-3 shows the simulation results for the droplet generation sequence for the T-junction at different time intervals.

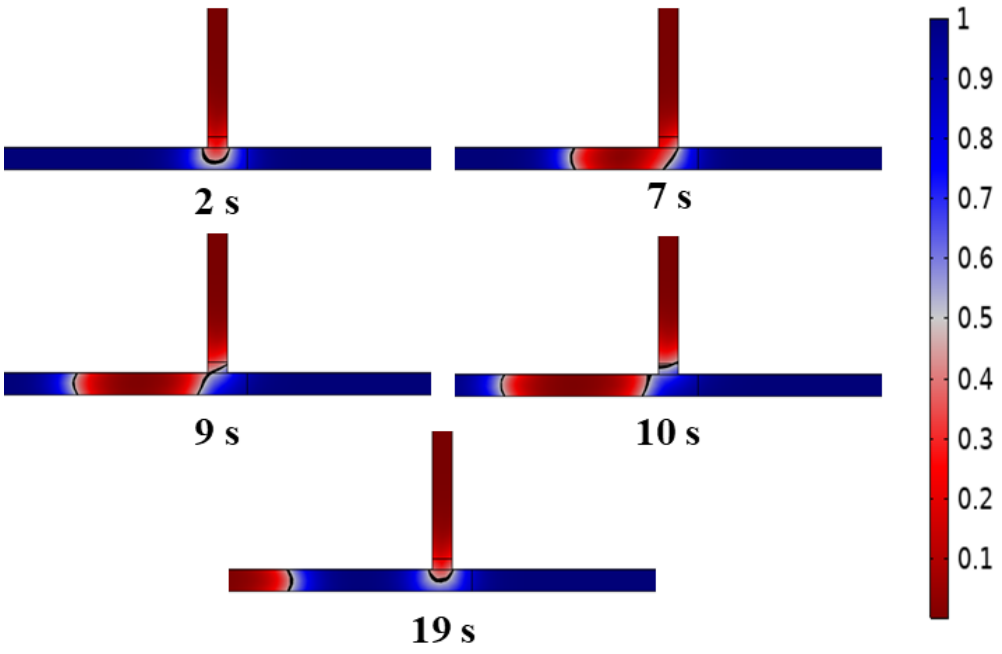

Figure 2-3: Numerical simulation results showing the necking and droplet generation processes at the T-junction. The red outline represents the interface between two immiscible fluids.

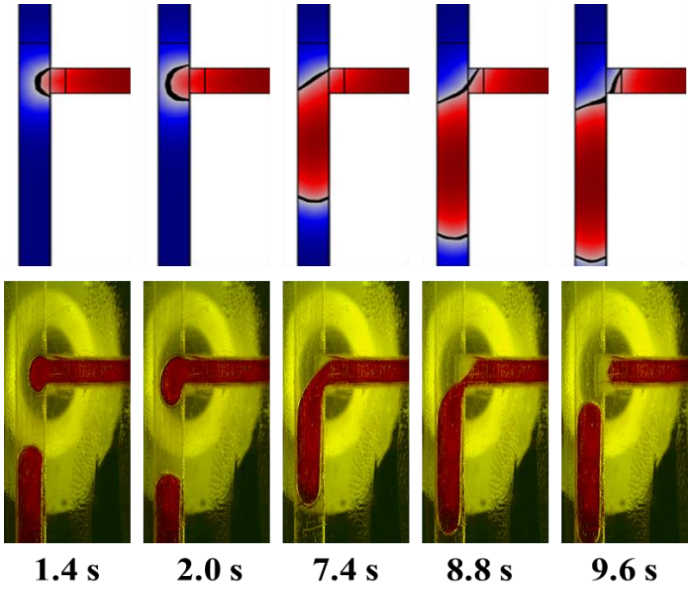

Figure 2-4: Comparison of numerical (top) and experimental (bottom) results showing the breaking up of the droplet from dispersed fluid in T-junction at different time intervals.

The simulation is performed to understand droplet break-up at the T-junction because the droplet breakup process provides information about the optimum values concerning fluid velocity, channel dimension, and fluid viscosity. If the design geometry and flow rates are not optimized before the fabrication, then jetting and/or irregular droplet sizes will result. Numerical results show that a flow rate of 0.1 ml/min for both fluids and a channel aspect ratio of 1.11:1 will create consistent droplets of 3.5 mm in size. In T-junction there will be three distinct flow regimes: squeezing, tearing, or dripping, and jetting. The droplet size dependence can be described by the dimensionless number capillary number (Ca=$\mu u/\gamma$) [55] which depends on the viscosity (μ), average flow velocity (u), and the interfacial tension (γ) between two immiscible fluid. In the T-junction, squeezing is observed at lower Ca levels, and as the Ca increases it shifts from squeezing to dripping, then jetting. The squeezing regime can be seen in both numerical simulation and experimental, as the Ca for our model is in the lesser range of 0.0007 [56]. Figure 2-4 shows a comparison between experimental and numerical results for different time stamps. The dispersed fluid at the interface changes its flow direction at 1.4 s. There is a sharp curve at the front of a droplet when it starts moving in the channel due to increased velocity, which can be seen at 2.0 s. The velocity increase is caused by the merging of the continuous fluid and dispersed fluids [57]. At 7.4 s, the dispersed fluid fills the width of the channel by obstructing the flow which increases the pressure at the junction and starts flowing downstream with the continuous fluid. There is a change in pressure between the front side of the droplet and the rear side of it which pushes the droplet further by creating a necking process that begins at 8.8 s, where the dispersed fluid at the intersection starts to thin out this is due to the interfacial tension which tries to reduce the surface area of the dispersed fluid. The difference in pressure at the 2.0 s is 31.03 Pa [58], [59] and at the time of 8.8 s, it's 12.78 Pa. Finally, a fragment portion of dispersed fluid breaks apart, forming a

droplet, as can be seen at 9.6 s. The numerical simulation showed that as the flow of dispersed fluid is increased, it started to block the channel and reduce continuous flow by restricting it. Then a change in the flow direction of the dispersed fluid started to move downstream of the channel, and as it moved to form a droplet, the necking area began to decrease and finally cut off. The research found that the channel width of 2 mm and the depth of 1.8 mm are suitable from the simulation of the mineral oil as continuous fluid and the DI water as a dispersed fluid, and this is then adapted to the prototype design.

FABRICATION

The design consists of a multilayer comprising the T-junction in the bottom layer, an adhesive seal in the middle layer, and a pneumatic chamber in the top layer as shown in Figure 2-5. To control the pneumatic pressure inside the chamber, laser cutting is used. Because of its rigidity, ease of fabrication with laser cutting, and optical transparency, the polymethyl methacrylate (PMMA) material is considered. The fabrication process involved in the droplet generator and its assembling can be seen in Figure 2-5 (a-e).

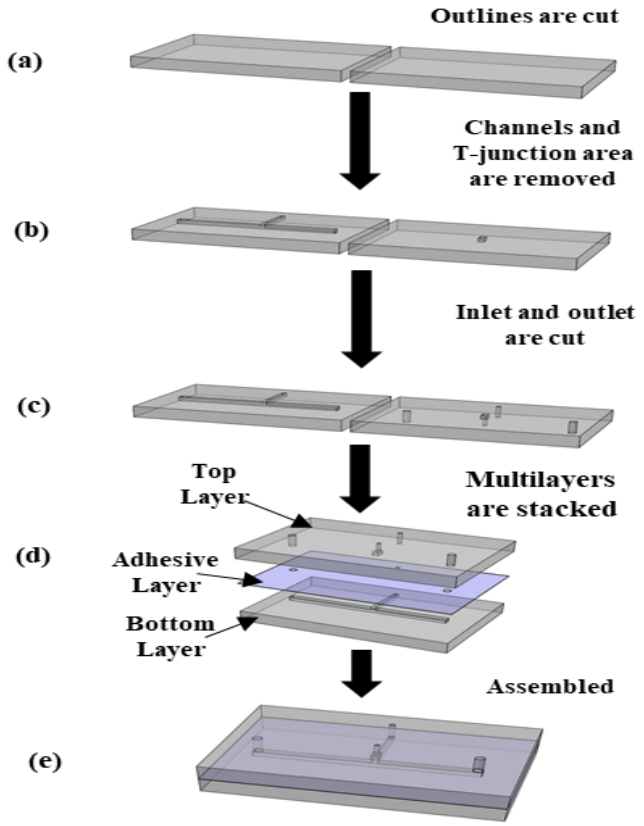

Figure 2-5: Fabrication process and assembly: (a) Laser cutting of the outline, (b) T-junction channels and pneumatic chamber are removed with laser machining, (c) inlet and outlet channels in the top layer are cut using a laser, (d) three layers, which will be assembled by stacking on top of another, and (e) the assembled model.

Polymethyl methacrylate (PMMA) material (both top and bottom layers) of 6 mm thickness along with a sheet of an adhesive seal (middle layer) of 0.2 mm from BIO-RAD [60] are utilized for making the droplet generator. Distilled water, colored with food dye, is used as the dispersed fluid due to its good optical visibility. To prevent mixing, mineral oil is employed as a continuous fluid.

The fabrication process is carried out using a laser cutter/engraver due to its rapidity, ease, and cost-effectiveness, making it a good option for mass production. A sheet of PMMA is taken for

the fabrication and, both the top and bottom layers are cut simultaneously to shorten the fabrication time by half. Figure 2-5 (a) shows the first step where the outline of the droplet generator is cut into a PMMA sheet, which roughly takes about 0.5 to 1.0 min depending on the size of the model. The T-junction and the pneumatic chamber of 2.6×1.6 mm dimension is simultaneously created see Figure 2-5 (b), which took up to 2.0 to 4.0 mins and may vary depending on the complexities of the pattern needed to be patterned. The pneumatic chamber and the T-junction have the same depth of 1.8 mm. After removing the material for the pneumatic chamber and the horizontal channels for the T-junction, the vertical circular channels are cut in the top layer and even this step takes up about 0.5 to 1.0 mins. The vertical channel consists of the inlet for the T-junction, as well as the pneumatic chamber and the outlet for the T-junction, as shown in Figure 2-5 (c). Here, the T-junction has two vertical channel inlets, one for dispersed fluid and another for continuous fluid. After the individual layers are manufactured, a bio seal layer is used to seal off the top T-junction while also acting as an adhesion layer to keep the top and bottom layers together. The bonded multi-layer is then kept in a bench vice for about 25.0 to 30.0 mins to improve adhesion. The model is then punched for inlets and outlets on the top layer's surface to connect with ports. Figure 2-5 (d) shows the individual layers that are later assembled, one on top of the other, to make the complete chip. The three layers are stacked so that the adhesive layer is sandwiched between the top and bottom layers. The top layer of the model consists of the inlet and outlet channels of the T-junction, the pneumatic chamber inlet, and the chamber itself. The bottom layer consists of a T-junction for droplet generation. The pneumatic chamber is at the bottom of the top layer, one end having an inlet channel and the other open area being sealed by the adhesive seal. The adhesive seal has holes for the inlet and outlet channel for the T-junction. The adhesive seal layer acts as

both a fluid leak sealant and a flexible membrane reacting to the pneumatic pressure. Figure 2-5 (e) shows the assembled droplet generator.

PROTOTYPE TESTING

Prototypes were fabricated and tested for characterizing the performance of the pneumatic control system. In the research experiments are performed by changing the pressure inside the pneumatic system to regulate droplet size. Figure 2-6 shows the experimental setup used for droplet generation, and size regulation, consisting of syringe pumps, pneumatic pressure line, pressure gauge, and digital microscope. The dispersed fluid and continuous fluid are pumped to the droplet generator with the help of a syringe pump (Harvard Apparatus Pump 11). Another InfusionONE syringe pump (Darwin Microfluidics) for pneumatic control is integrated as in Figure 2-6 (a). As in Figure 2-6 (b) the schematic representation of the setup is shown where two syringe pumps are considered, one just to pump dispersed and continuous fluid at the same flow rate and the other one to maintain pneumatic pressure inside the chamber. A pressure gauge is connected to the fluidic line between the syringe pump and the pneumatic chamber to monitor the pressure maintained inside the chamber during droplet regulation. So, with this pneumatic pressure, in the research were able to regulate the droplet size by the deflection of a flexible membrane. A digital microscope (the Dino-Elite) was placed on top of the T-junction to capture the droplet generation sequence. This digital microscope is connected to the computer as a visual aid. The pressure in the pneumatic chamber is recorded using a pressure gauge.

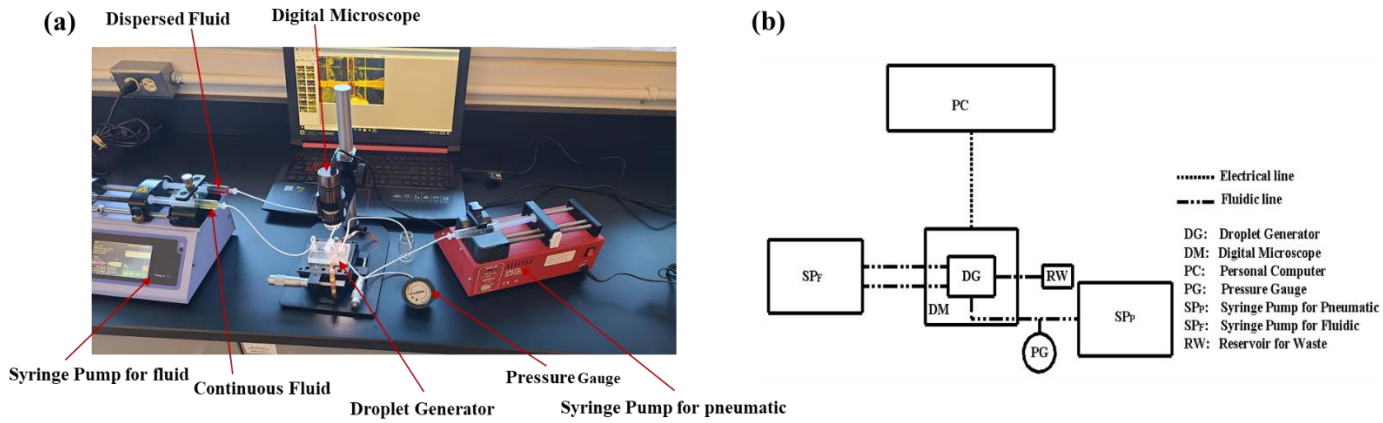

Figure 2-6: The Experimental setup used for droplet regulation, (a) the whole setup, and (b) schematic representation of the setup.

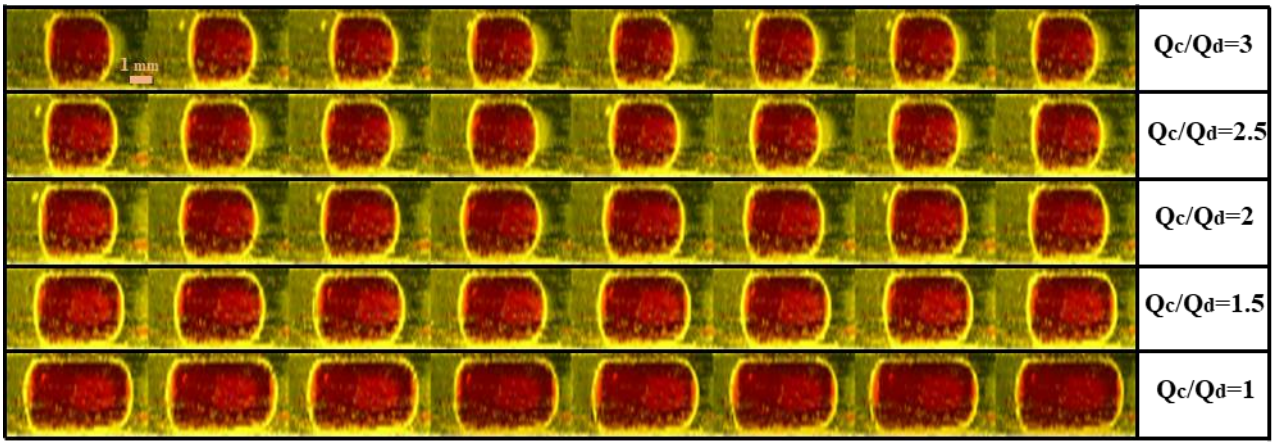

Figure 2-7: Droplet size control by utilizing only flow ratio at the T-junction. A sequence of images shows different droplet sizes for different flow rate ratios. Qc is the flow rate of continuous flow and Qd is the flow rate of dispersing fluid.

The DI water which is dyed with food color (contains Propylene glycol, Tartrazine, and Propylparaben) has been taken as dispersed fluid and the mineral oil (contains 97% naphthenic oil). In the syringe pump, the dispersed and continuous fluids are set at the same flow rate. In the classical method, the droplets are regulated by changing the flow rates between the continuous

fluid and dispersed fluid, and, thus, two pumps are required. To compare the droplet size generated for the pneumatic pressure and the conventional method, in the research experiment was conducted by changing the flow rates using the conventional method. For the droplet regulation, used two separate syringe pumps for individual fluids. In one the constant flow rate of 0.1 ml/min for dispersed fluid was set. For continuous fluid, the flow rate from 0.1 to 0.3 ml/min in an increment of 0.05 ml/min with the aid of another syringe pump is increased. As the flow rate of the continuous fluid increased the droplet size started to decrease. Figure 2-7 shows the different droplet sizes generated for different flow rate ratios. Here, Qc is the flow rate of a continuous fluid, and Qd is the flow rate of a dispersed fluid. In the experiment, Qd was kept constant, while Qc was varied.

REGULATION OF DROPLET SIZE

As mentioned earlier, classical droplet generators use differential flow rates between dispersed and continuous fluids to regulate droplet sizes. To achieve this, a secondary pump is needed to maintain the differential flow rate between them and an additional continuous fluid to maintain the size of the regulated droplet. The droplet size is reduced by increasing the flow rate of the continuous fluid. To eliminate the need for additional continuous fluid usage, a pneumatic chamber is created above the T-junction, shown in, Figure 2-8 (a). Figure 2-8 (b) shows the side view when the flexible membrane is not deflected.

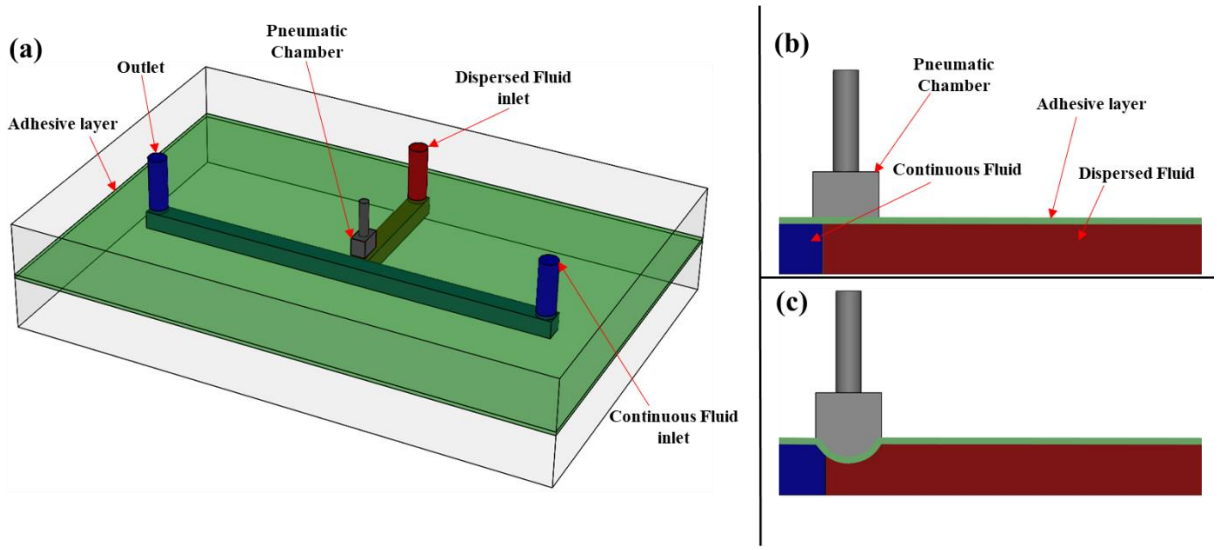

Figure 2-8: (a) Orthographic view of the T-junction and the pneumatic chamber inside the droplet generator, (b) the side view where there is no pressure inside the chamber, and (c) the side view when there is pressure inside the chamber.

As explained earlier, an adhesive seal functioning as a flexible membrane separates the pneumatic chamber and the T-junction which can be seen in Figure 2-8 (a). The adhesive layer has just three holes that are punched just for the inlet for dispersed and continuous fluid, and another hole is for the outlet of the droplet generated. So, by pumping more pneumatic air into the chamber with the syringe pump, it begin to raise the pneumatic pressure within the chamber. The fluidic line is connected to the pressure gauge, which aids in monitoring the pressure inside the pneumatic chamber. The pressure inside the chamber is increased until it reaches the desired pneumatic pressure. The pressure inside the chamber begins to exert force on the surface as the pressure rises. There would be no significant deformation because the material for the droplet generator is PMMA, which is rigid in nature. Then the pressure force acts on the flexible membrane's surface, causing it to deform. The flexible membrane starts to deflect as the pressure within the chamber increases, reducing the area of the dispersed fluid at the junction; see Figure 2-8 (c). As mentioned

earlier, the flow area will be restricted to the dispersed fluid channel with the aid of the adhesive layer to regulate the droplet size by regulating the dispersed flow without increasing any of the flow rates. The volume rate decreases as the cross-sectional area of the dispersed fluid decrease at the interface. The size of the generated droplet decreases as the volume flow rate decreases, compared to earlier droplet generation.

COMPARISON OF REGULATED DROPLET SIZE WITH AND WITHOUT PNEUMATIC

To characterize the performance of the pneumatic control system, experiments were performed by varying the pressure and monitoring the droplet size. The droplet size decreased with the increase in the applied pressure. Figure 2-9 consists of the images of the droplet at different applied pressure. Figure 2-9 (a) shows the largest droplet generated without pneumatic pressure application, which has been used as a reference droplet for further study. With incremental pneumatic pressure of 0.1 MPa, the droplet sizes decreased, as depicted by Figure 2-9 (b), (c), (d), and (e).

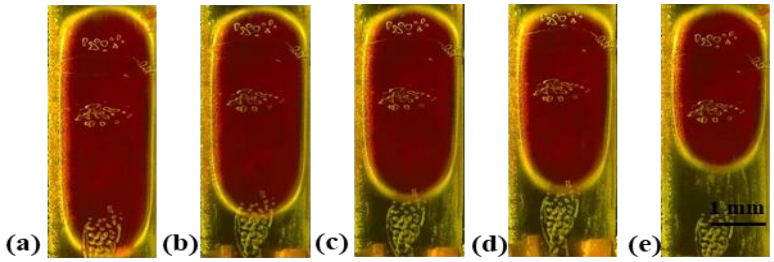

Figure 2-9: The size of droplets generated with and without the application of pneumatic pressure, (a) Without the application of pneumatic pressure and with pneumatic pressure of, (b) 0.1 MPa, (c) 0.2 MPa, (d) 0.3 MPa, and (e) 0.4 MPa.

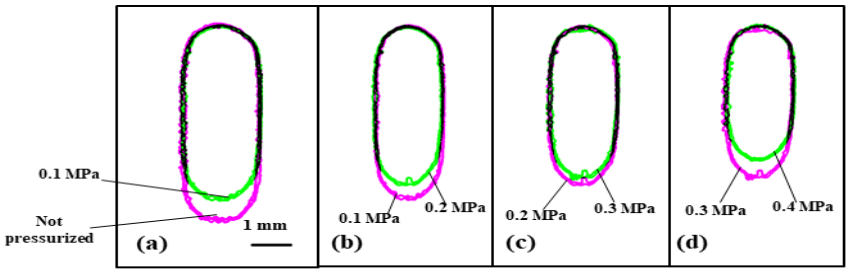

Figure 2-10: The comparison of droplet sizes, for pneumatic pressure of (a) 0 to 0.1 MPa, (b) 0.1 MPa to 0.2 MPa, (c) 0.2 MPa to 0.3, (d) 0.3 MPa to 0.4 MPa.

To quantify the size of the droplet, image analysis was performed to trace the two-dimensional droplet boundary. The traced boundaries of two consecutive applied pressure cases are stacked on top of each other to clearly show the difference, see Figure 2-10. Figure 2-10 (a) compares droplets generated with 0.1 MPa (green-colored) with that without applied pneumatic pressure (pink-colored) where the flow rates for both continuous and dispersed were 0.1 ml/min. Similarly, Figure 2-10 (b), (c), (d) shows the comparison for droplets generated at successive pneumatic pressures. The decrease in droplet size with increasing pneumatic pressure over the tested range is sure.

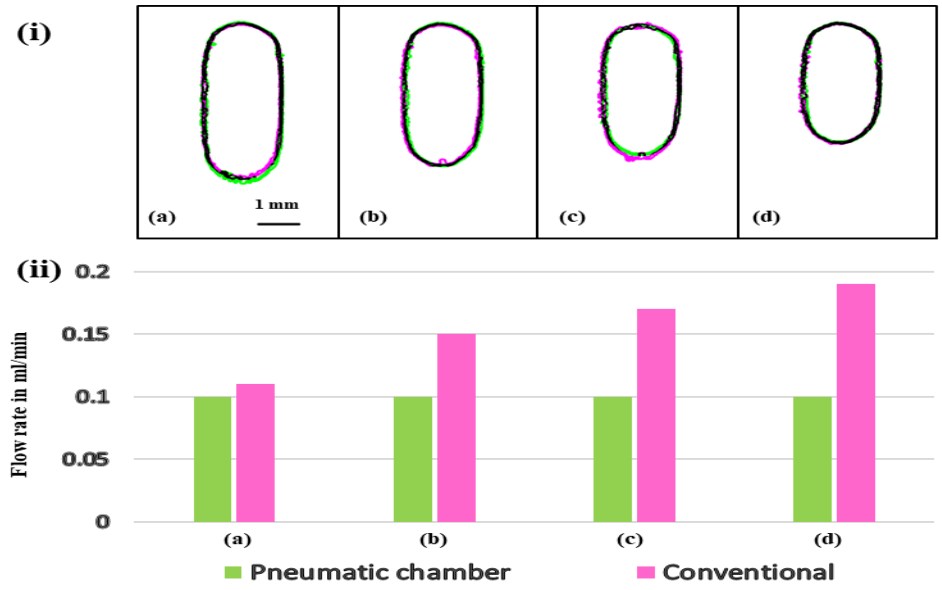

Figure 2-11: (i) The comparison of droplet sizes between different oil flow rate and applied pneumatic pressure, (a) 0.11 ml/min and 0.1 MPa, (b) 0.15 ml/min and 0.2 MPa, (c) 0.17 ml/min and 0.3 MPa and (d) 0.19 ml/min and 0.4 MPa, and (ii) the bar chart comparison of continuous fluid flow rate between conventional model and pneumatic chamber model.

As discussed earlier, the conventional practice to decrease the droplet size is to increase the continuous fluid flow rate, Figure 2-11 (i) compares droplet sizes generated by the conventional method with that by controlling the pneumatic pressure. For the pneumatic pressure control experiment, the flow rate has been kept at 0.1 ml/min for both fluids, while altering the pneumatic pressure. For the experiment using the conventional method, the flow of the dispersed fluid is kept constant at 0.1 ml/min, the continuous fluid was increased in increments of 0.01 ml/min.

Figure 2-11 (i) (a) compares the droplet generated using 0.1 MPa pneumatic pressure in the novel method with that produced by the conventional method with 0.11 ml/min of continuous fluid flow. Similarly, Figure 2-11 (i) (b), (c) and (d) compare the droplets generated at successive pneumatic pressures and continuous fluid flow rates. Figure 2-11 (i) (d) corresponds to the case where the

applied pneumatic pressures were 0.4 MPa and 0.19 ml/min of continuous flow rate. In other words, to generate the said droplet size using the conventional method, an extra 0.09 ml of continuous fluid is needed every min. Figure 2-11 (ii) shows the bar chart of the flow rate of continuous fluid in both the pneumatic chamber model and the conventional model. Figure 2-11 (ii) (a), (b), (c) and (d) are the flowrates of the models at the time of the droplet production as in Figure 2-11 (i) (a), (b), (c) and (d).

Before comparing droplet regulation between the pneumatic pressure method and the traditional method, an uncertainty error analysis was carried out to understand and calculate the variance of values from its mean value. The area of the droplet is determined based on the number of pixels in the 2D droplet in this situation. As a result, in this thesis, an image analysis was performed using MATLAB, with the reference droplet pixel area acting as a standard to which other droplets were compared using a percentage comparison of the reference droplet area. As a result, in the pneumatic pressure system, 10 number of droplets (n) are considered for analysis for each pressure value, and the average, standard deviation, and uncertainty error calculated values are shown in Table 2. Using the formula below, the average value (y_m) of the droplet area based on pixel number is calculated first. This value is then converted to a percentage by comparing it to the reference droplet area pixels. The standard deviation (Sm) formula is then used to measure the variance of the values from the average value. To understand the deviation between the values from the average values, the uncertainty error (σ) was determined using the formula below. Calculations are performed in the same way for the conventional method to determine the average value, standard deviation, and uncertainty error, as shown in Table 3 where the number of droplets (n) considered is 5.

$$y_m = \frac{1}{n}\sum_{i=1}^{n} y_i \quad (4)$$

$$\mathrm{Sm} = \sqrt{\sum_{i=1}^{n} \frac{(y_i - y_m)^2}{n-1}} \quad (5)$$

$$\sigma = \frac{Sm}{\sqrt{n}} \quad (6)$$

Table 2: The uncertainty error study for the pneumatic pressure method experimental results.

Pneumatic pressure method				
Pressure (MPa)	**Average pixels (y_m)**	**Percentage area (%)**	**Root mean square (Sm)**	**Uncertainty error (σ)**
0.10	31480.70	85.60	9.22	$\pm$2.92
0.20	28388.00	77.19	4.25	$\pm$1.34
0.30	26042.60	70.82	6.61	$\pm$2.09
0.40	22998.20	62.54	5.41	$\pm$1.71

Table 3: The uncertainty error study for the conventional method experimental results.

Conventional method				
Flow rate (ml/min)	Average Pixels (y_m)	Percentage area (%)	Root mean square (Sm)	Uncertainty error (σ)
0.11	46177.80	88.18	9.34	$\pm$4.18
0.12	42875.00	81.88	4.64	$\pm$2.08
0.13	41190.00	78.66	5.33	$\pm$2.38
0.14	40808.60	77.93	5.69	$\pm$2.54
0.15	40644.00	77.62	4.95	$\pm$2.22
0.16	40632.40	77.59	4.92	$\pm$2.20
0.17	37342.20	71.31	13.90	$\pm$6.22
0.18	34593.00	66.06	16.00	$\pm$7.16
0.19	32648.20	62.35	5.58	$\pm$2.49

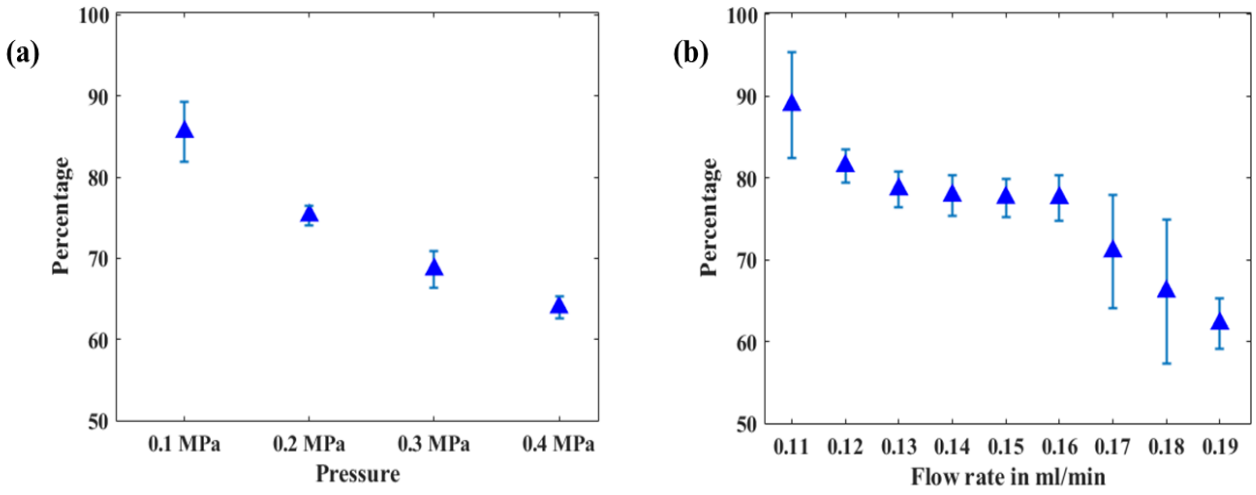

Figure 2-12: Percentage area change in droplet size (with respect to reference droplet), (a) with increasing pneumatic pressure, and (b) with increasing continuous fluid flow rate.

Figure 2-12 shows the graph of droplet's 2-dimensional cross-sectional area percentage decrease for (a) the new pneumatic-pressure method, and (b), the conventional method. Here the droplet is considered which is the droplet size generated for the initial condition of both fluid flow rates of 0.1 ml/min as reference droplet size as mentioned earlier. To reduce the droplet size by 38% the flow rate of the continuous fluid must be significantly heightened to 0.19 ml/min in the conventional method, whereas 0.4 MPa pneumatic pressure can be applied in the new method to obtain the same small droplets.

In this research a pneumatic chamber is included because our goal was to regulate the droplet without additional usage of continuous fluid. The multilayer design was developed using a rapid manufacturing laser cutting process and the pneumatic chamber operates at the T-junction interface. When the pressure inside the pneumatic chamber was 0.4 MPa, the model was able to reduce the droplet size by up to 38 percent when compared to a reference droplet. Also experimented with droplet regulation using traditional differential flow rates to investigate continuous fluid consumption. Then discovered that the droplet size generated in our model for 0.4 MPa pressure is the same as the one generated in the traditional model with an increased continuous fluid flow rate of 0.19 ml/min, which showed that in the traditional method additional 0.09 ml of continuous fluid for every minute is required to maintain that droplet size. Further to the droplet regulation, some applications require information on the fluid concentration in a droplet, so in the following chapter, will integrate a capacitor-based sensor to detect, quantify, and characterize the generated droplets.

CHAPTER 3

DESIGN AND DEVELOPMENT OF ELECTRICAL SENSING AND CHARACTERIZING OF DROPLETS

For precise control over droplet generation, after the generation of droplets, there is a need to automatically sense and monitor the droplet's size, composition, and speed. One way of monitoring is by using an optical method, which is usually done in real-time with the aid of microscope imaging, capturing time-lapse images or videos, and processing images to calculate the number of droplets generated [61]. Optical detection is the most frequently used approach for microfluidics detection and has been designed specifically for fluorescence, chemiluminescence, diffraction, absorption, and variation of the refractive index [62], [63]. To detect the generated droplets, these systems have both the off-chip method and the on-chip method. For the off-chip process, additional optical equipment such as high-speed charge-coupled device (CCD) cameras and microscopes that have low background signal levels are used. On-chip optical detection techniques require both fluidic elements and optical elements to be integrated, such as movable mirror arrays, refractive microlenses, optical filters, and so on [64]. In other sensing methods, paramagnetic material is added to the dispersed fluid, so the generated droplets are sensible for the magnetic sensors [65]. Whereas in the electro-chemical [66], [67] the sensing method is based on the reaction of fluids with the electrodes; these reactions produce a differential ion charge at the integrated electrodes [44].

Quantifying the generated droplets and measuring the output quantity and characterizing a droplet is important, and one way to do it on-chip is by using integrated electrodes for capacitive sensing that can offer ease of implementation [68], [69]. A capacitive-based sensor uses capacitance

variance to detect droplets due to changes in a dielectric material. In capacitive sensing, 3D-printed devices with embedded electrodes for measuring the size of droplets showed promise in integrating electrodes in 3D-printed droplet generators [70]. Integrating electrodes after printing the 3D-printed devices is a challenge due to access required inside the device, as well as the non-compatibility of metal during printing in most of the processes. The methods used for capacitive-based sensors often use a common structure called a finger electrode or an interdigital electrode [71], [72]. In interdigitated capacitive sensing multiple electrodes are often required, which has shown greater promising performance in electro-wetting-based droplet manipulation techniques, and these series of electrodes are positioned in the channel for performing a complex integration. To keep it simple, only used a pair of electrodes to quantify and characterize the generated droplets as a capacitive-based sensor.

In this chapter, a capacitive sensing method using two electrodes along the wall in a laser-cut T-junction droplet generator is presented. A simple electrode integration, where a thin copper foil (electrodes) is added to two sides of the wall to form a capacitor for capacitive sensing is presented. The capacitance of a capacitor can be determined by $C = \frac{\varepsilon_0 \varepsilon_r A}{d}$, where ε_0 is the vacuum permittivity (F/m), ε_r is the relative static permittivity of the dielectric, A is the overlap area (m^2), and d is the distance between the parallel plates (m). For a fixed pair of electrodes, all the geometric parameters are constant, and thus, the capacitance varies with ε_r, which is a function of the passing material. In other words, the capacitance varies from continuous fluid to dispersed fluid as the droplet moves between the electrodes. Using this principle, can quantify the droplets generated at the output. In this study, utilized two electrodes along fluidic channel walls to characterize droplet material and size in conjunction with droplet size control.

In the earlier chapter, a pneumatically controllable T-junction droplet generator that is capable of varying the junction area vertically to control droplets is presented. The pneumatic pressure chamber placed on top of the junction provides additional control over droplets; this could be beneficial for further development of cost-effective microdroplet research and development. In the next section, will discuss the details of the numerical simulation of droplet generation. That will be followed by an outline of device structures and fabrication methods. Finally, will present prototype performance and characterization.

Before considering fabrication and experimentation, developed and utilized a numerical simulation to design and geometry and position of the electrode pair. In the research first will present the proposed design of our sensing method, and then the numerical simulation and electrode design. Following that, will explain the experimental setup and procedure, and then detail the analysis. Lastly, will present both the control and sensing methods. In this research used a pneumatic control [73] to characterize the size, so the output speed of the droplet remained nearly constant, and focused on differentiating droplets of different sizes with the capacitance sensor here.

In a classical T-junction design, Figure 3-1 depicts the formation of droplets at the interface. In our proposed design the dispersed fluid flows perpendicularly to the continuous fluid until the two fluids cross at the T-junction. As the dispersed fluid begins to change direction at the interface, the continuous fluid shears it into capture-shaped droplets. After the droplet is formed, it flows down the same channel along with the continuous fluid. These droplets are then quantified using the electrode capacitance variation due to the dielectric material change that is integrated into the continuous fluidic channel.

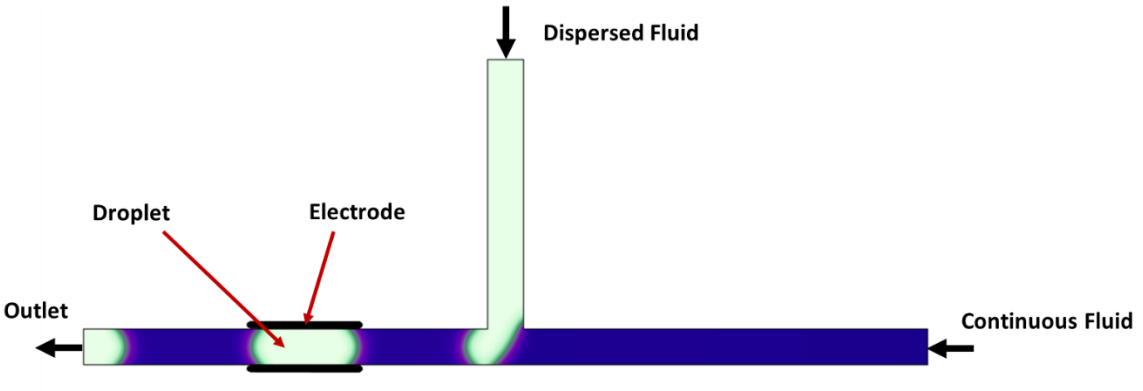

Figure 3-1: Schematic showing the conceptual design for quantification and characterization of the droplets via a capacitive sensor.

NUMERICAL SIMULATION

To understand the formation of a droplet in a T-junction, a numerical model is created to explore how flow and geometric parameters affect the formation of droplets and how the sensor quantifies these changes. Simulation and modeling of droplet generation in a T-junction have been studied extensively [52], [73], [74]. Have not seen any studies that simultaneously model and measure droplet generation up till now based on the knowledge of studied literature in similar applications. It is important to model the real-time sensing and generation together to determine the best width of the electrodes and understand the expected sensing characteristics as well as limitations of the design. By simulating these parameters prior to fabrication, will be able to use the most efficient space, which is important in microfluidics where the scale is minimized as much as possible. Knowing the design's limitations like minimum electrode width and distance from T-junction helps us to verify the numerical model with the experimental model. We used COMSOL 5.5 V to simulate our model. The fine mesh was used in this thesis to simulate and understand the effects of integrated electrodes on the generated droplet movement, as shown in Figure 3-2.

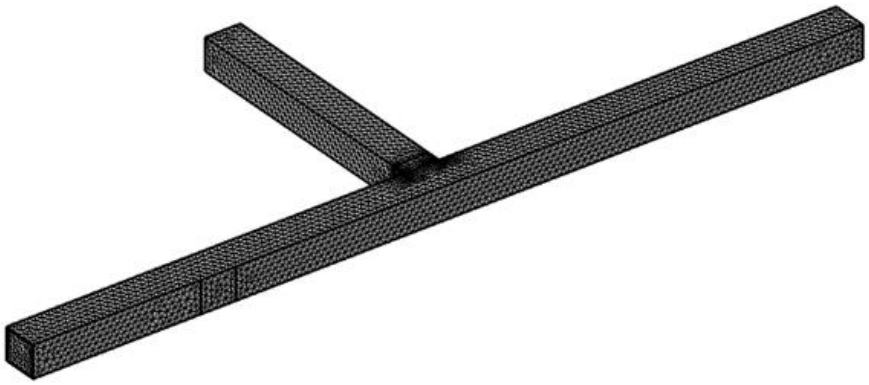

Figure 3-2: The meshing sizes considered during numerical simulation for the T-junction flow channels with integrated electrode.

In this research invoked two multiphysics solvers, the first being the laminar two-phase flow, phase-field physics, to solve for the fluid flow and the droplet formations. For resolving the involved fluid motion, called upon Navier-Stokes's equation and continuity equation:

$$\rho\frac{\partial u}{\partial t} + \rho(u \cdot \nabla)u = \nabla \cdot [-pI + \mu(\nabla u + (\nabla u)^T)] + F_{St} + \rho g + F \quad 7$$

$$\nabla \cdot u = 0 \quad 8$$

where u is velocity (m/s), ρ is density (kg/m^3), μ is dynamic viscosity (Pa-s), p is pressure (Pa), I is the identity matrix, g is gravity (m/s^2), F_{St} is a surface tension force (N/m^3), and F is an additional volume force (N/m^3). The droplet formation was simulated using a phase-field interface where the phase field variable (Φ) was set, that is,

$$\frac{\partial \phi}{dt} + u \cdot \nabla \phi = \nabla \cdot \frac{3\chi\sigma\varepsilon}{2\sqrt{2}} \nabla \Psi \quad (9)$$

$$\Psi = -\nabla \cdot \varepsilon^2 \nabla \phi + (\phi^2 - 1)\phi \quad (10)$$

For the two immiscible fluids, set the phase field variable of the continuous and dispersed fluids to -1 and 1, respectively. Here, σ is the surface tension coefficient (N/m), ε is a numerical parameter (m) that defines the thickness of the fluid interface, and χ controls the mobility of the interface. The second multiphysics solver invoked is electrostatics, which is used to measure capacitance using the formula below,

$$-\nabla \cdot (\varepsilon_0 \varepsilon_r \nabla V) = 0 \quad (11)$$

Here, V is the electric potential, ε_0 is the permittivity of vacuum, and ε_r is the relative permittivity. All the above equations were automatically set when the laminar two-phase flow, phase-field, and electrostatics multiphysics for our model is considered. In this research used Maxwell's stress tensor with the electric force to couple the two solvers is considered, that is,

$$T = \begin{bmatrix} Txx & Txy & Txz \\ Tyx & Tyy & Tyz \\ Tzx & Tzy & Tzz \end{bmatrix} \quad (12)$$

$$= \begin{bmatrix} \varepsilon_0\varepsilon_r E_x^2 - \frac{1}{2}\varepsilon_0\varepsilon_r\left(E_x^2 + E_y^2 + E_z^2\right) & \varepsilon_0\varepsilon_r E_x E_y & \varepsilon_0\varepsilon_r E_x E_z \\ \varepsilon_0\varepsilon_r E_y E_x & \varepsilon_0\varepsilon_r E_y^2 - \frac{1}{2}\varepsilon_0\varepsilon_r\left(E_x^2 + E_y^2 + E_z^2\right) & \varepsilon_0\varepsilon_r E_y E_z \\ \varepsilon_0\varepsilon_r E_z E_x & \varepsilon_0\varepsilon_r E_z E_y & \varepsilon_0\varepsilon_r E_z^2 - \frac{1}{2}\varepsilon_0\varepsilon_r\left(E_x^2 + E_y^2 + E_z^2\right) \end{bmatrix}$$

The volume forces in the x, y, and z directions were calculated by the divergence of a tensor. These volume forces were added to the laminar flow physics in the simulation where the force vectors were replaced by F_x, F_y, and F_z respectively, where the value

$$F = \nabla \cdot T \quad (13)$$

$$F_x = \frac{\partial Txx}{\partial x} + \frac{\partial Txy}{\partial y} + \frac{\partial Txz}{\partial z} \quad (14)$$

$$F_y = \frac{\partial Tyx}{\partial x} + \frac{\partial Tyy}{\partial y} + \frac{\partial Tyz}{\partial z} \quad (15)$$

$$F_z = \frac{\partial Tzx}{\partial x} + \frac{\partial Tzy}{\partial y} + \frac{\partial Tzz}{\partial z} \quad (16)$$

Here used two electrodes as a capacitor at the end channel of the T-junction, and then set one of the electrodes as a terminal electrode with a set voltage of 1V and the other one as a ground electrode. The continuous fluid flowed between the electrodes of the dielectric material except when the droplet moved between them, which caused a change in the capacitance. Figure 3-3 shows the movement of droplets between the electrodes and the legend represents the phase difference between two fluids. Figure 3-3 (a) shows the T-junction and capacitor when the continuous fluid, the dielectric material, is passing between the electrodes. Figure 3-3 (b) depicts the droplet between the electrodes where the capacitor senses the passing dispersed fluid.

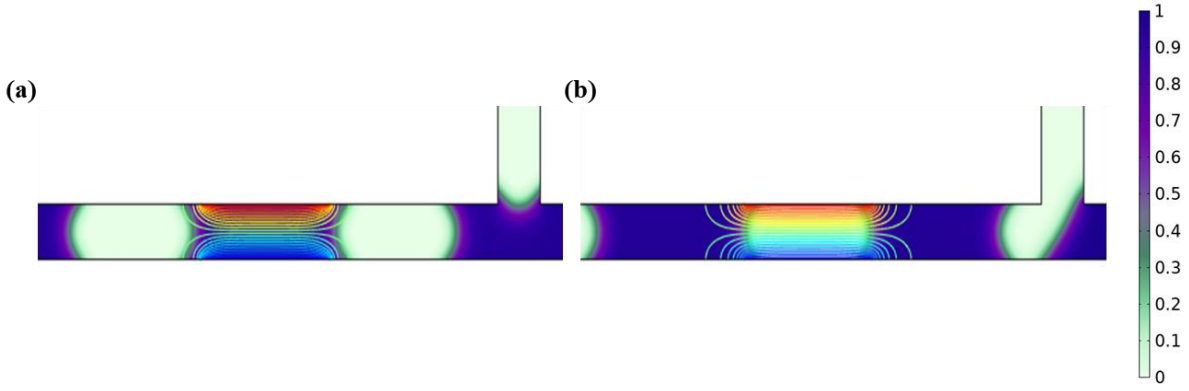

Figure 3-3: Droplet movement (from right to left) between the capacitor electrodes. The green color at the edge of the droplet denotes the droplet interface and the colored contour plot shows the electrical field across the sensor

As explained earlier, capacitance is a function of the dielectric material between the electrodes. The change of the dielectric material from continuous fluid to dispersed fluid causes a change in the capacitance. Using this principle, can quantify the number of droplets formed. Figure 3-4 portrays a series of numerical simulation iterations for deducing the optimum electrode distance from the T-junction and its width for better sensitivity. Here the electrode position is increased from next to the T-junction as shown in Figure 3-4 (a) until the minimum capacitance value for continuous fluid was reached at around 2 mm, beyond which it decreased negligibly with further increase in distance. Have considered more than 2 mm value for experimentation to get a better visual with negligible image noise such as inlet and outlet fittings, so it can be used to verify the capacitance value. Next, sought the optimal size of the electrode. Therefore, modified the width of the electrode from 0 to 8 mm and found that the maximum value obtained for the dispersed fluid was associated with 6 mm electrode width, as shown in Figure 3-4 (b). Consequently, in this research set the width of the electrode at 6 mm.

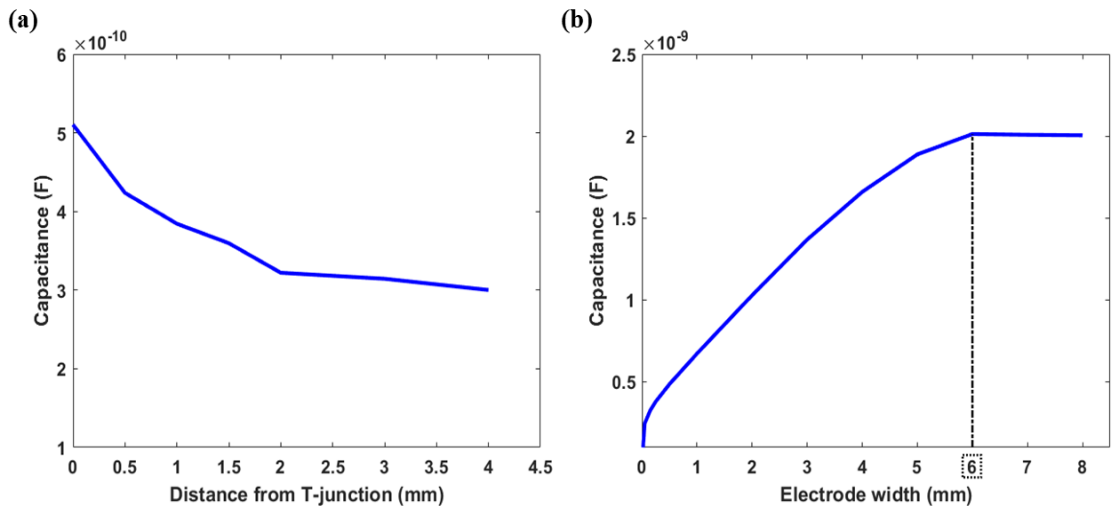

Figure 3-4: Capacitance value obtained in numerical simulation as increased, (a) the distance from T-junction until it reaches minimum value for continuous fluid, and (b) width of electrode until it reaches a maximum value for dispersed fluid.

EXPERIMENTAL SETUP

Prototypes were fabricated and tested for characterizing the performance of the pneumatic control system. Here will be performing experiments by changing the pressure inside the pneumatic system to regulate droplet size. Details of the manufacturing of the T-junction droplet generator with pneumatic control have been presented in our previous chapter, here integrated electrodes downstream for sensing and control. The model layers were fabricated using a laser cutter and then assembled. The model had three layers, with PMMA as both the top and bottom layers, sandwiched in between was an adhesive layer that served as a flexible membrane for pneumatic pressure and for holding the top and bottom layers together. Figure 3-5 shows the experimental setup and the assembled model used for testing. For visual assistance, the experimental setup as shown in Figure 3-5 (a) includes a digital microscope (the Dino-Elite) connected to a computer. This microscope is employed to verify the droplet measurement using the capacitive-based sensor. Utilized a

syringe pump (Harvard Apparatus Pump 11) for pumping both dispersed fluid and continuous fluid. Used an E4980A Precision LCR meter (Agilent) as part of the sensor integrated within the droplet generator and connected to a computer to get real-time data. The schematic representation of the experimental setup used for droplet detection is shown in Figure 3-5 (b). Integrated a copper strip which acts as capacitive-based electrode as depicted in Figure 3-5 (c) as a sensor for quantifying and characterizing the droplet formed. The cross-sectional view of the droplet generator with the integrated sensor is shown in Figure 3-5 (d).

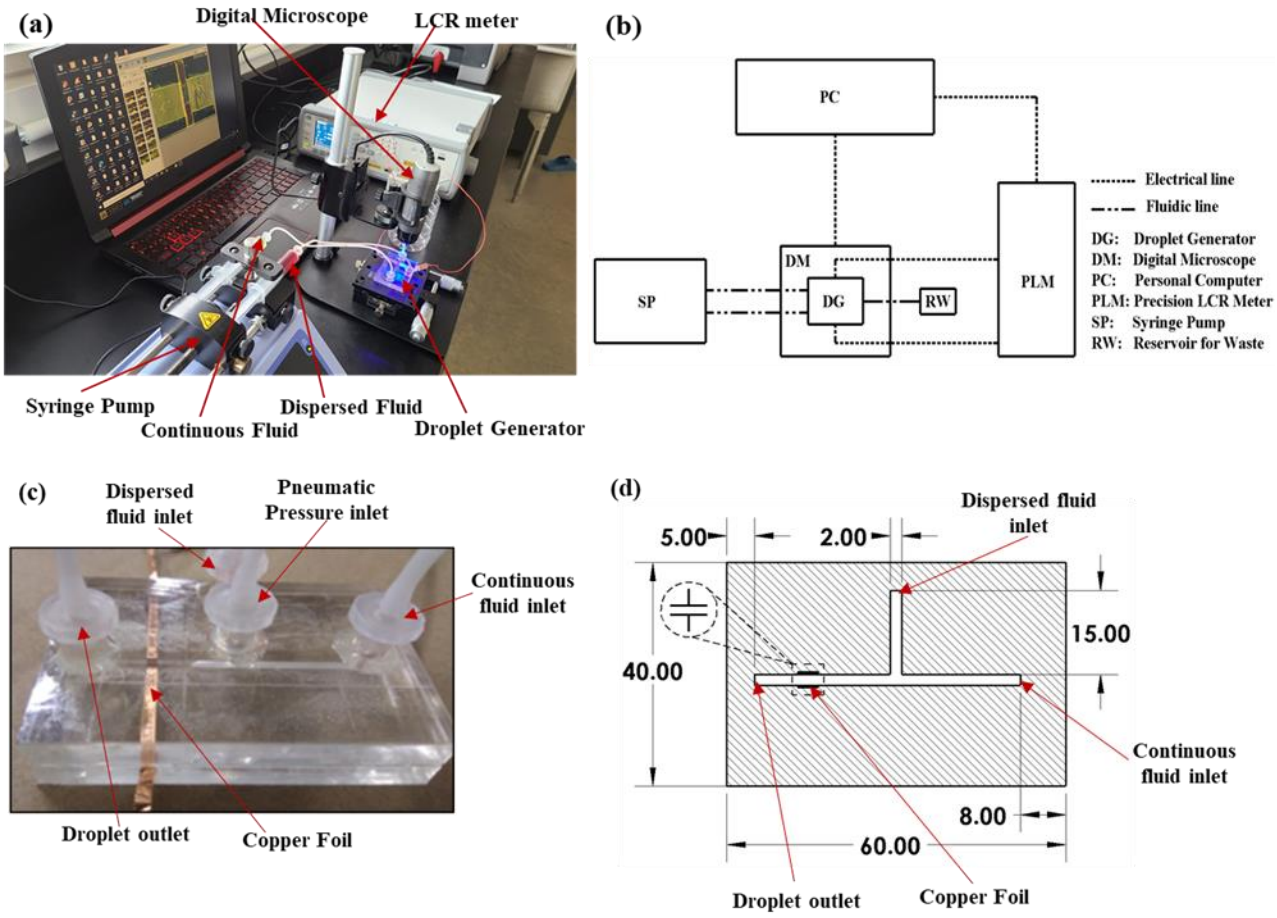

Figure 3-5: Experimental setup (a) the experimental setup, (b) schematic of the whole setup, (c) the assembled model, and (d) cut-sectional view of the model with integrated sensor (dimensions are in mm).

EXPERIMENTAL RESULTS

The general methods used in the channel to detect droplet movement are the optical method or the electrical detection method via electrodes. In the optical method, a light source that passes through the transparent channel enables detection. The droplet detection works on the principle of the differential refractive index between fluids flowing through the channel. Electrochemical reactions between fluid and electrode occur when an electric field is applied in the electrode method. The dispersed fluid and continuous fluid react with the electrode to create differential electrical output; this differential is used to quantify the number of droplets generated. Used copper foil as the capacitor electrodes integrated into the system as shown in Figure 3-5 (c). As explained earlier, the variation in capacitance depends on the relative static permittivity of the dielectric (ε_r). The value of ε_r for water is 80 and for oil it is 3 [75]. As such, the capacitance value is lower when the continuous fluid is in the gap, and it increases when dispersed fluid (droplet) enters the passage. In this research the electrodes are connected to an LCR meter; see Figure 3-5.

Integrated the capacitor electrodes with the droplet generator to quantify the droplets generated. Figure 3-6 shows the variation in capacitance as the droplet enters and passes through the section embraced by the electrodes with a flow rate of 0.1 ml/min for both dispersed fluid and continuous fluid. The capacitance value was around 1.96 PF as seen in Figure 3-6 (a) when there is continuous fluid between electrodes, and it begins to increase with the approaching dispersed fluid (droplet) and reaches a maximum value of 2.31 PF when the droplet is fully positioned between electrodes. So, using this capacitance variation to material change at the output at any given time, were able to quantify the generated droplets, and in our model, were able to generate 7 droplets for 28.7 seconds, as shown in Figure 3-6 (b). The capacitance variance for seven droplets is not uniform, but rather has a slight variation, which is due to a ±2 difference in generated droplet area.

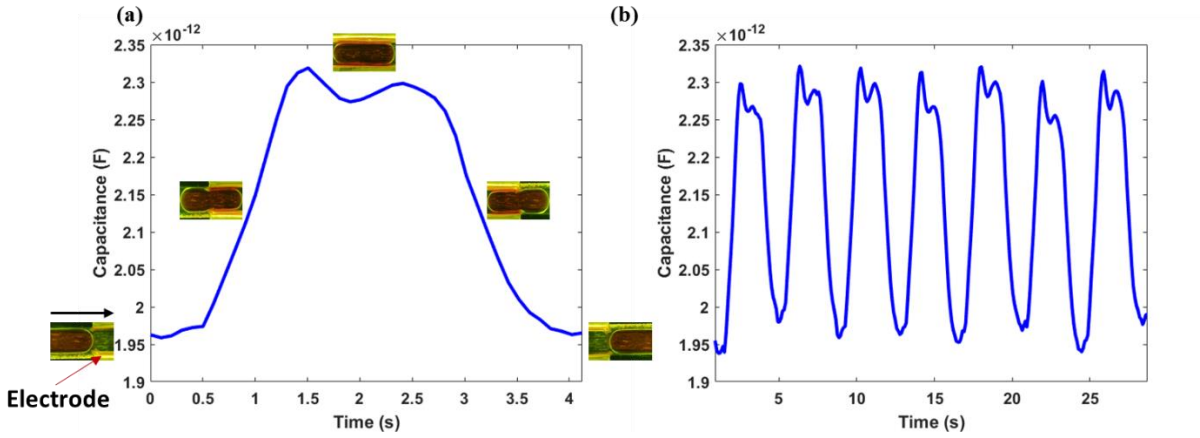

Figure 3-6: The variation in capacitance obtained as a function of droplet movement between electrodes for, (a) a single droplet (from left to right), and (b) a series of 7 droplets over 28.7 seconds at a flow rate of 0.1 ml/min.

Also employed the integrated model to characterize the droplet based on the dispersed material, and the result obtained can be seen in Figure 3-7. Here performed two different experiments for the same length of time and flow rate of 0.1 ml/min to understand how capacitance variations differ when the dispersed material is altered. Here the droplet generated for both conditions have the same droplet size, so any difference in capacitance variation generated between them is mainly because of the material change. For the first experiment, used DI water colored with food dye and the results obtained can be seen in Figure 3-7 (a). The capacitance for continuous fluid is about 1.96 PF and it reaches a value of 2.31 PF when a dispersed fluid (DI water) droplet enters between the electrodes. Used a salt solution with a molarity of 3.093 M for the second experiment, and the results obtained can be seen in Figure 3-7 (b), where the capacitance is about 1.78 PF for the continuous fluid, and it reaches 3.19 PF for the dispersed fluid (salt solution) droplet. Owing to the difference in the electrical properties of the dispersed material, the capacitance sensed in a real-

time analysis for dispersed fluid increases by 38.1 percent, while the capacitance for continuous fluid decreases by 9.2 percent when the dispersed fluid is changed from DI water to salt solution.

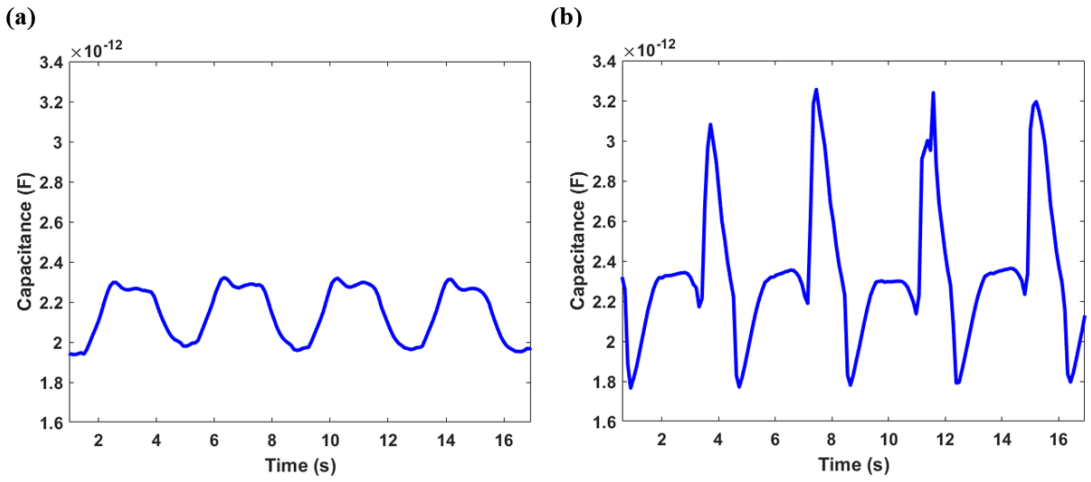

Figure 3-7: The variation in capacitance for droplet movement between electrodes with different dispersed material, (a) DI water, and (b) salt solution, at a flow rate of 0.1 ml/min.

The pneumatic chamber on top of the T-junction [38] regulates the droplet size, allowing us to reduce the droplet size without the additional usage of continuous fluid or increasing the flow rate as in the conventional method. So, used the pneumatic chamber to generate droplets of various sizes, and the size (cross-sectional area) difference between the droplets is shown in Figure 3-8. Two conditions are shown: one where the droplets are generated without pressurization, and the other where the pressure inside the chamber is 0.1 MPa. For both conditions, the flow rate was kept constant at 0.1 ml/min, and seven consecutive droplets were considered. Figure 3-8 (a) shows the size difference graph for both conditions, with an uncertainty of ±2 percentage. For unpressurized conditions, the generated droplet size is maximum, so the average size generated for this condition has been considered as a reference droplet for further analysis. The droplet size for pressurized condition decreased by 9.7 percent relative to the reference droplet, as pressure

inside the chamber is increased to 0.1 MPa. The difference in average size for the generated droplets of these two conditions can be seen in Figure 3-8 (b).

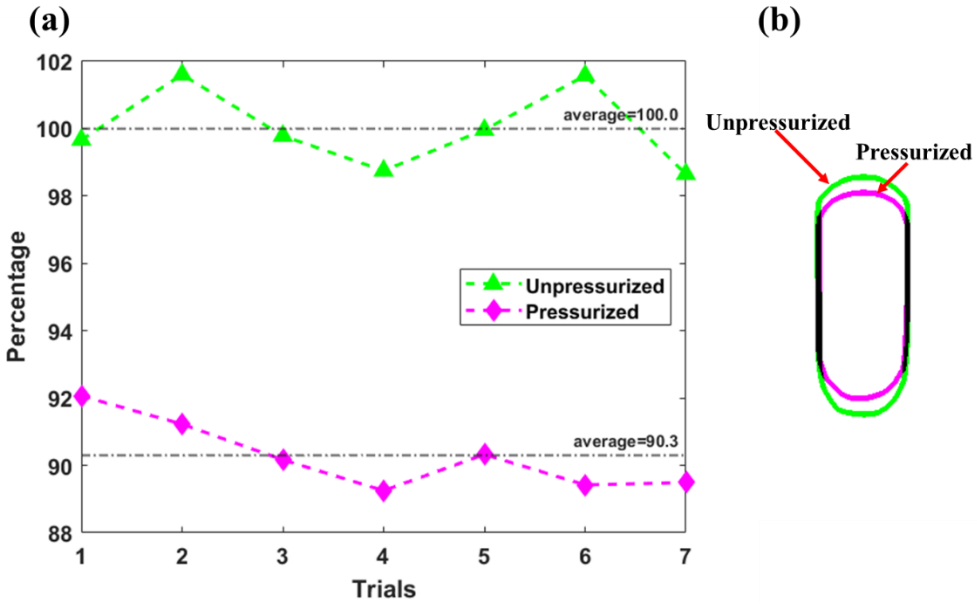

Figure 3-8: Variation in droplet size (cross-sectional area) formed without and with the aid of pneumatic pressure, (a) droplet size versus trial number, and (b) the comparison of average droplet size between the two conditions.

Have considered seven consecutive droplets for both conditions to understand how the variation in capacitance responds when there is a decrease in droplet size. For the two studied conditions, Figure 3-9 depicts the variation in capacitance generated by the respective seven consecutive droplets discussed earlier. Figure 3-9 (a) depicts the variation in capacitance for the unpressurized condition, whereas Figure 3-9 (b) shows the result for the pressurized case. For the unpressurized condition, the average capacitance values for the continuous fluid and dispersed droplets are 1.96 PF and 2.31 PF, respectively. These values are respectively 2.0 PF and 2.20 PF for the pressurized case. Thus, the capacitance for dispersed fluid decreases by 4.7 percent, while that of a continuous fluid increases by 2.0 percent as the droplet cross-sectional area decreases by 9.7 percent relative

to the reference droplet area. The difference in capacitance values between the two conditions is due to the probability that in a pressurized condition, the droplet size decreases, and when that reduced droplet is fully positioned between the electrodes in real-time analysis, the proportion of dispersed material sensed is relatively lower than in an unpressurized condition, and the continuous fluid takes up that reduced space involuntarily. As a result of this change, the dispersed fluid capacitance value decreases, while the continuous fluid capacitance value increases as the droplet size reduce. So, if the variation in capacitance of any produced droplets falls into one of the above two categories, so can easily characterize them to their specific condition. This allows us to determine how many droplets are formed for both conditions and characterize them accordingly with the aid of integrated copper electrodes as a capacitor.

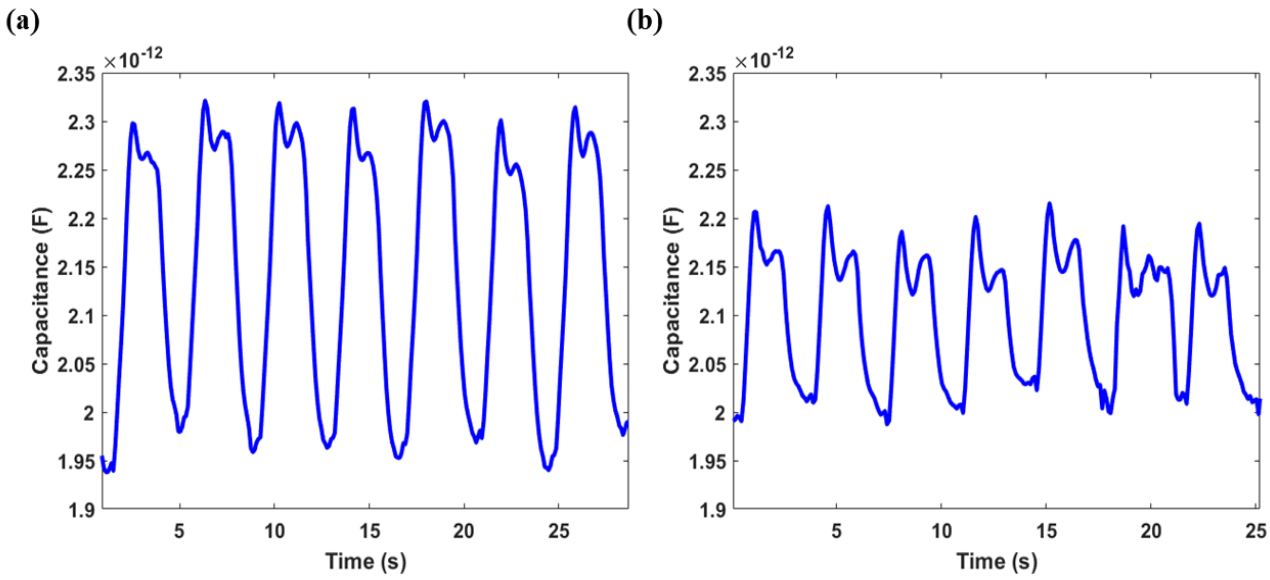

Figure 3-9: The variation in capacitance for two conditions, (a) without pneumatic pressure, and (b) with pneumatic pressure inside the chamber.

Used a simple capacitor-based electrode to quantify and characterize the droplets based on their size and materials in the fluidic channels. The capacitance values of the capacitor-based sensor

vary when the dielectric material between the capacitor is altered while all other values stay unchanged. So were able to quantify the generated droplets using this principle, and in our experiment, the model was able to generate seven droplets in 28.7 seconds. To characterize droplets based on material, used two different dispersed materials, one being DI water and the other being a salt solution. As a result, as the dispersed material was varied, the capacitance variance for droplet movement varied. Then, to characterize droplets based on size, used our novel pneumatic control method to regulate droplet size. When 0.1 MPa pressure was achieved inside the chamber, the droplet size decreased by 9.7% relative to the reference droplet. The capacitance variance for the droplet movement varied in the real-time analysis as a result of this size variance. The detection and characterization of the generated droplets could be done in chemical analysis-based applications using this simple integrated capacitive-based sensor.

CHAPTER 4

CONCLUSIONS

A T-junction-based microdroplet generator have been designed to improve droplet size control. The pneumatic-based control mechanisms developed in this thesis eliminates the need for challenging continuous fluid manipulation for droplet size control. Which requires complicated flow control and additional continuous fluid for controlling the generated droplet size. To overcome this a pneumatic chamber operating at the T-junction interface is proposed and demonstrated. Experimental results confirmed the fidelity of the new design in regulating the droplet size. Our results show the reduction in droplet size is proportional to an increase in pressure inside the pneumatic chamber. The new design can easily reduce the droplet size by 38% compared to the reference droplet generated with no pressure. This means a significant percentage of droplet size control is available for a constant flow rate using a pneumatic chamber. In this reaeacrh proposed and demonstrated a simple electrode interfacing in the fluidic channels so that the generated droplets can be quantified, controlled, and characterized using capacitive sensing. As the variation in capacitance depends on the change in a dielectric material, were able to use this phenomenon to quantify the droplets generated. Our results showed that were able to quantify seven droplets generated for 28.7 seconds using repeated waves of variation in capacitance for their respective droplet movement. Then, based on the materials of the fluid and the droplet size, the capacitive-based sensor was used to characterize droplets. There was a notable shift in the material-based capacitive variance for the two different materials that was used as the dispersed fluid, which helped to differentiate them. Then used a pneumatic control to regulate the droplet to characterize them based on size. Therefore, there would be no significant droplet velocity variation

in the produced droplet for two conditions that would affect sensing. As a result of the pneumatic control, were able to reduce the droplet size, resulting in a decrease in capacitance for the dispersed fluid and an increase for the continuous fluid. This is due to the change in the proportion of material sensed between electrodes for both fluids as the droplet size decreased in real-time analysis. In conclusion, the thesis have given a simple capacitive-based sensor that can be easily incorporated during manufacturing into a droplet generator that could be used to quantify and characterize the generated droplet. Besides, the multi-layer design is compatible with rapid and cost-effective manufacturing, optically transparent, and droplet regulators. To this end, have provided a simplified droplet generator design with size control that is suited for mass production via desktop-based laser cutting, which is rapid and cost-effective to fabricate. As discussed earlier, different concentration droplets are needed for protein crystallization and study of drug dose-response, which is accomplished using the conventional method. Here our model could be implemented, which would use pneumatic control to regulate the concentration of droplets and a capacitor-based sensor to characterize the different concentration droplets.

FUTURE WORK

Our research was divided into two streams: one focused on the regulation of droplets using pneumatic pressure, and the other on the quantification and characterization of materials and sizes using a capacitive-based sensor. Currently experimented with a chamber on top of a T-junction in droplet regulation with pneumatic control. More research into the location and positioning of this chamber to see how it affects droplet regulation could be done. The fluid used in the pneumatic chamber is air, which can be altered to a different viscous fluid to see how it affects the regulated droplet size. In the case of a capacitive sensor, different materials with electrical properties could

be used as dispersed material to better understand the capacitive-based sensor. A micromixer could be used to create multiple liquid concentrations, which could then be used to create droplets of different concentrations to see how they react with the capacitive sensor. Particles could be incorporated into the droplets, enabling research to find how a foreign particle within the droplet affects capacitive sensor sensing.

REFERENCES

[1] K. E. Petersen, “Fabrication of an Integrated, Planar Silicon Ink-Jet Structure,” IEEE Trans. Electron Devices, vol. 26, no. 12, p. p 1918-1920, Dec. 1979, doi: 10.1109/T-ED.1979.19796.

[2] A. Manz, N. Graber, and H. M. Widmer, “Miniaturized total chemical analysis systems: A novel concept for chemical sensing,” Sens. Actuators B Chem., vol. 1, no. 1–6, pp. 244–248, Jan. 1990, doi: 10.1016/0925-4005(90)80209-I.

[3] D. J. Beebe, G. A. Mensing, and G. M. Walker, “Physics and Applications of Microfluidics in Biology,” Annu. Rev. Biomed. Eng., vol. 4, no. 1, pp. 261–286, Aug. 2002, doi: 10.1146/annurev.bioeng.4.112601.125916.

[4] Q. Xiao, Y. Ji, Z. Xiao, Y. Zhang, H. Lin, and Q. Wang, “Novel multifunctional NaYF4:Er3+,Yb3+/PEGDA hybrid microspheres: NIR-light-activated photopolymerization and drug delivery,” Chem. Commun., vol. 49, no. 15, p. 1527, 2013, doi: 10.1039/c2cc37620b.

[5] H.-C. Hsu, L.-M. Chu, B. Liu, and C.-Y. Lai, “Design on MEMS-based 3D biochip for drug-released dispenser,” Microsyst. Technol., vol. 23, no. 2, pp. 355–360, Feb. 2017, doi: 10.1007/s00542-015-2594-4.

[6] L. Wang, “Gold Nanoparticle-based Optical Probes for Target-Responsive DNA Structures,” Gold Bull., vol. 41, no. 1, pp. 37–41, 2008, doi: 10.1007/BF03215621.

[7] L. Zhang, Q. Feng, J. Wang, J. Sun, X. Shi, and X. Jiang, “Microfluidic Synthesis of Rigid Nanovesicles for Hydrophilic Reagents Delivery,” Angew. Chem. Int. Ed., vol. 54, no. 13, pp. 3952–3956, Mar. 2015, doi: 10.1002/anie.201500096.

[8] P. Tirandazi and C. H. Hidrovo, “An integrated gas-liquid droplet microfluidic platform for digital sampling and detection of airborne targets,” Sens. Actuators B Chem., vol. 267, pp. 279–293, Aug. 2018, doi: 10.1016/j.snb.2018.03.057.

[9] N. Shembekar, C. Chaipan, R. Utharala, and C. A. Merten, “Droplet-based microfluidics in drug discovery, transcriptomics and high-throughput molecular genetics,” Lab. Chip, vol. 16, no. 8, pp. 1314–1331, 2016, doi: 10.1039/C6LC00249H.

[10] L. Li and R. F. Ismagilov, “Protein Crystallization Using Microfluidic Technologies Based on Valves, Droplets, and SlipChip,” Annu. Rev. Biophys., vol. 39, no. 1, pp. 139–158, Apr. 2010, doi: 10.1146/annurev.biophys.050708.133630.

[11] B. Zheng, J. D. Tice, L. S. Roach, and R. F. Ismagilov, “A Droplet-Based, Composite PDMS/Glass Capillary Microfluidic System for Evaluating Protein Crystallization Conditions by Microbatch and Vapor-Diffusion Methods with On-Chip X-Ray Diffraction,” Angew. Chem. Int. Ed., vol. 43, no. 19, pp. 2508–2511, May 2004, doi: 10.1002/anie.200453974.

[12] O. J. Miller et al., “High-resolution dose-response screening using droplet-based microfluidics,” Proc. Natl. Acad. Sci., vol. 109, no. 2, pp. 378–383, Jan. 2012, doi: 10.1073/pnas.1113324109.

[13] M. J. Ahamed, S. I. Gubarenko, R. Ben-Mrad, and P. Sullivan, “A Piezoactuated Droplet-Dispensing Microfluidic Chip,” J. Microelectromechanical Syst., vol. 19, no. 1, pp. 110–119, Feb. 2010, doi: 10.1109/JMEMS.2009.2036866.

[14] M. J. Ahamed, R. Ben-Mrad, and P. Sullivan, “A Drop-on-Demand-Based Electrostatically Actuated Microdispenser,” J. Microelectromechanical Syst., vol. 22, no. 1, pp. 177–185, Feb. 2013, doi: 10.1109/JMEMS.2012.2221681.

[15] Z. Mao, K. Yoshida, and J. Kim, “Developing O/O (oil-in-oil) droplet generators on a chip by using ECF (electro-conjugate fluid) micropumps,” Sens. Actuators B Chem., vol. 296, p. 126669, Oct. 2019, doi: 10.1016/j.snb.2019.126669.

[16] U. Demirci and M. Toner, “Direct Etch Method for Microfluidic Channel and Nano-Height Post Fabrication by Picoliter Droplets,” in 19th IEEE International Conference on Micro Electro Mechanical Systems, Istanbul, Turkey, 2006, pp. 326–329, doi: 10.1109/MEMSYS.2006.1627802.

[17] A. Agarwal, A. Salahuddin, H. Wang, and M. J. Ahamed, “Design and development of an efficient fluid mixing for 3D printed lab-on-a-chip,” Microsyst. Technol., vol. 26, no. 8, pp. 2465–2477, Aug. 2020, doi: 10.1007/s00542-020-04787-9.

[18] L. Yang, L. Zhu, Z. Li, and B. Lu, “A liquid molding method for the fabrication of microfluidic devices based on a drop-on-demand generation of patterned substrates,” Microsyst. Technol., vol. 23, no. 10, pp. 4543–4551, Oct. 2017, doi: 10.1007/s00542-016-3242-3.

[19] L. Donvito, L. Galluccio, A. Lombardo, G. Morabito, A. Nicolosi, and M. Reno, "Experimental validation of a simple, low-cost, T-junction droplet generator fabricated through 3D printing," J. Micromechanics Microengineering, vol. 25, no. 3, p. 035013, Mar. 2015, doi: 10.1088/0960-1317/25/3/035013.

[20] J. M. Zhang, A. A. Aguirre-Pablo, E. Q. Li, U. Buttner, and S. T. Thoroddsen, "Droplet generation in cross-flow for cost-effective 3D-printed 'plug-and-play' microfluidic devices," RSC Adv., vol. 6, no. 84, pp. 81120–81129, 2016, doi: 10.1039/C6RA11724D.

[21] Z. Jiao, L. Zhao, C. Tang, H. Shi, F. Wang, and B. Hu, "Droplet-based PCR in a 3D-printed microfluidic chip for miRNA-21 detection," Anal. Methods, vol. 11, no. 26, pp. 3286–3293, 2019, doi: 10.1039/C9AY01108K.

[22] H. V. Nguyen, H. Q. Nguyen, V. D. Nguyen, and T. S. Seo, "A 3D printed screw-and-nut based droplet generator with facile and precise droplet size controllability," Sens. Actuators B Chem., vol. 296, p. 126676, Oct. 2019, doi: 10.1016/j.snb.2019.126676.

[23] S. Yadavali, H.-H. Jeong, D. Lee, and D. Issadore, "Silicon and glass very large scale microfluidic droplet integration for terascale generation of polymer microparticles," Nat. Commun., vol. 9, no. 1, p. 1222, Dec. 2018, doi: 10.1038/s41467-018-03515-2.

[24] T. Glawdel, C. Elbuken, and C. L. Ren, "Droplet formation in microfluidic T-junction generators operating in the transitional regime. I. Experimental observations," Phys. Rev. E, vol. 85, no. 1, p. 016322, Jan. 2012, doi: 10.1103/PhysRevE.85.016322.

[25] K. Loizou, W. Thielemans, and B. N. Hewakandamby, "Effect of Geometry on Droplet Generation in a Microfluidic T-Junction," in Volume 2, Fora: Cavitation and Multiphase Flow; Fluid Measurements and Instrumentation; Microfluidics; Multiphase Flows: Work in Progress, Incline Village, Nevada, USA, Jul. 2013, p. V002T21A003, doi: 10.1115/FEDSM2013-16161.

[26] W. Zeng, S. Li, and Z. Wang, "Closed-loop feedback control of droplet formation in a T-junction microdroplet generator," Sens. Actuators Phys., vol. 233, pp. 542–547, Sep. 2015, doi: 10.1016/j.sna.2015.08.002.

[27] B. Charlot, D. Coudouel, F. Very, P. Combette, and A. Giani, "Droplet generation for thermal transient stimulation of pyroelectric PZT element," Sens. Actuators Phys., vol. 225, pp. 103–110, Apr. 2015, doi: 10.1016/j.sna.2015.02.011.

[28] W. Fan et al., “High efficiency single-cell capture based on microfluidics for single cell analysis,” J. Micromechanics Microengineering, vol. 29, no. 3, p. 035004, Mar. 2019, doi: 10.1088/1361-6439/aaf9df.

[29] J. M. Chen, M.-C. Kuo, and C.-P. Liu, “Control of Droplet Generation in Flow-Focusing Microfluidic Device with a Converging-Diverging Nozzle-Shaped Section,” Jpn. J. Appl. Phys., vol. 50, no. 10, p. 107301, Oct. 2011, doi: 10.1143/JJAP.50.107301.

[30] S. Ghosh, G. Kamalakshakurup, A. P. Lee, and C. H. Ahn, “A mass manufacturable thermoplastic based microfluidic droplet generator on cyclic olefin copolymer,” J. Micromechanics Microengineering, vol. 29, no. 5, p. 055009, May 2019, doi: 10.1088/1361-6439/ab0e60.

[31] Y. Wu, X. Qian, M. Zhang, Y. Dong, S. Sun, and X. Wang, “Mode Transition of Droplet Formation in a Semi-3D Flow-Focusing Microfluidic Droplet System,” Micromachines, vol. 9, no. 4, p. 139, Mar. 2018, doi: 10.3390/mi9040139.

[32] F. Bai, X. He, X. Yang, R. Zhou, and C. Wang, “Three dimensional phase-field investigation of droplet formation in microfluidic flow focusing devices with experimental validation,” Int. J. Multiph. Flow, vol. 93, pp. 130–141, Jul. 2017, doi: 10.1016/j.ijmultiphaseflow.2017.04.008.

[33] W. Li et al., “Simultaneous generation of droplets with different dimensions in parallel integrated microfluidic droplet generators,” Soft Matter, vol. 4, no. 2, pp. 258–262, 2008, doi: 10.1039/B712917C.

[34] N. Gallah, N. Habbachi, and K. Besbes, “Design and modelling of droplet based microfluidic system enabled by electroosmotic micropump,” Microsyst. Technol., vol. 23, no. 12, pp. 5781–5787, Dec. 2017, doi: 10.1007/s00542-017-3414-9.

[35] P. Zhu, X. Tang, and L. Wang, “Droplet generation in co-flow microfluidic channels with vibration,” Microfluid. Nanofluidics, vol. 20, no. 3, p. 47, Mar. 2016, doi: 10.1007/s10404-016-1717-2.

[36] A. Shams Khorrami and P. Rezai, “Oscillating dispersed-phase co-flow microfluidic droplet generation: Multi-droplet size effect,” Biomicrofluidics, vol. 12, no. 3, p. 034113, May 2018, doi: 10.1063/1.5034473.

[37] L. Wu, X. Liu, Y. Zhao, and Y. Chen, “Role of local geometry on droplet formation in axisymmetric microfluidics,” Chem. Eng. Sci., vol. 163, pp. 56–67, May 2017, doi: 10.1016/j.ces.2017.01.022.

[38] J. Lian, X. Luo, X. Huang, Y. Wang, Z. Xu, and X. Ruan, “Investigation of microfluidic co-flow effects on step emulsification: Interfacial tension and flow velocities,” Colloids Surf. Physicochem. Eng. Asp., vol. 568, pp. 381–390, May 2019, doi: 10.1016/j.colsurfa.2019.02.040.

[39] E. Piccin, D. Ferraro, P. Sartori, E. Chiarello, M. Pierno, and G. Mistura, “Generation of water-in-oil and oil-in-water microdroplets in polyester-toner microfluidic devices,” Sens. Actuators B Chem., vol. 196, pp. 525–531, Jun. 2014, doi: 10.1016/j.snb.2014.02.042.

[40] Z. Shen, Y. Zou, and X. Chen, “An integrated microfluidic signal generator using multiphase droplet grating,” Microfluid. Nanofluidics, vol. 14, no. 5, pp. 809–815, May 2013, doi: 10.1007/s10404-012-1099-z.

[41] Y.-J. Yang, X. Feng, N. Xu, D.-W. Pang, and Z.-L. Zhang, “Generation of sub-femtoliter droplet by T-junction splitting on microfluidic chips,” Appl. Phys. Lett., vol. 102, no. 12, p. 123502, Mar. 2013, doi: 10.1063/1.4798510.

[42] C.-H. Yeh, Y.-C. Chen, and Y.-C. Lin, “Generation of droplets with different concentrations using gradient-microfluidic droplet generator,” Microfluid. Nanofluidics, vol. 11, no. 3, pp. 245–253, Sep. 2011, doi: 10.1007/s10404-011-0791-8.

[43] P. K. Shivhare, A. Prabhakar, and A. K. Sen, “Optofluidics based lab-on-chip device for in situ measurement of mean droplet size and droplet size distribution of an emulsion,” J. Micromechanics Microengineering, vol. 27, no. 3, p. 035003, Mar. 2017, doi: 10.1088/1361-6439/aa53cc.

[44] S. Gu et al., “A droplet-based microfluidic electrochemical sensor using platinum-black microelectrode and its application in high sensitive glucose sensing,” Biosens. Bioelectron., vol. 55, pp. 106–112, May 2014, doi: 10.1016/j.bios.2013.12.002.

[45] T. M. Squires and S. R. Quake, “Microfluidics: Fluid physics at the nanoliter scale,” Rev. Mod. Phys., vol. 77, no. 3, pp. 977–1026, Oct. 2005, doi: 10.1103/RevModPhys.77.977.

[46] C. N. Baroud and H. Willaime, “Multiphase flows in microfluidics,” Comptes Rendus Phys., vol. 5, no. 5, pp. 547–555, Jun. 2004, doi: 10.1016/j.crhy.2004.04.006.

[47] A. Günther and K. F. Jensen, “Multiphase microfluidics: from flow characteristics to chemical and materials synthesis,” Lab Chip, vol. 6, no. 12, pp. 1487–1503, 2006, doi: 10.1039/B609851G.

[48] J. Collins and A. P. Lee, “Control of serial microfluidic droplet size gradient by step-wise ramping of flow rates,” Microfluid. Nanofluidics, vol. 3, no. 1, pp. 19–25, Dec. 2006, doi: 10.1007/s10404-006-0093-8.

[49] C.-H. Yeh and Y.-C. Lin, “Micro-Systems and Nanotechnologies in ELISA and Droplet Generation Applications,” ECS Trans., vol. 50, no. 12, pp. 409–412, Mar. 2013, doi: 10.1149/05012.0409ecst.

[50] M. Shojaeian and S. Hardt, “Fast electric control of the droplet size in a microfluidic T-junction droplet generator,” Appl. Phys. Lett., vol. 112, no. 19, p. 194102, May 2018, doi: 10.1063/1.5025874.

[51] H.-W. Wu, Y.-C. Huang, C.-L. Wu, and G.-B. Lee, “Exploitation of a microfluidic device capable of generating size-tunable droplets for gene delivery,” Microfluid. Nanofluidics, vol. 7, no. 1, pp. 45–56, Jul. 2009, doi: 10.1007/s10404-008-0359-4.

[52] V.-L. Wong, K. Loizou, P.-L. Lau, R. S. Graham, and B. N. Hewakandamby, “Numerical studies of shear-thinning droplet formation in a microfluidic T-junction using two-phase level-SET method,” Chem. Eng. Sci., vol. 174, pp. 157–173, Dec. 2017, doi: 10.1016/j.ces.2017.08.027.

[53] M. Azarmanesh, M. Farhadi, and P. Azizian, “Simulation of the double emulsion formation through a hierarchical T-junction microchannel,” Int. J. Numer. Methods Heat Fluid Flow, vol. 25, no. 7, pp. 1705–1717, Sep. 2015, doi: 10.1108/HFF-09-2014-0294.

[54] M. Besanjideh, A. Shamloo, and S. Kazemzadeh Hannani, “Enhanced oil-in-water droplet generation in a T-junction microchannel using water-based nanofluids with shear-thinning behavior: A numerical study,” Phys. Fluids, vol. 33, no. 1, p. 012007, Jan. 2021, doi: 10.1063/5.0030676.

[55] I. Chakraborty, J. Ricouvier, P. Yazhgur, P. Tabeling, and A. M. Leshansky, “Droplet generation at Hele-Shaw microfluidic T-junction,” Phys. Fluids, vol. 31, no. 2, p. 022010, Feb. 2019, doi: 10.1063/1.5086808.

[56] X.-B. Li, F.-C. Li, J.-C. Yang, H. Kinoshita, M. Oishi, and M. Oshima, “Study on the mechanism of droplet formation in T-junction microchannel,” Chem. Eng. Sci., vol. 69, no. 1, pp. 340–351, Feb. 2012, doi: 10.1016/j.ces.2011.10.048.

[57] W. Zeng, S. Li, and H. Fu, “Modeling of the pressure fluctuations induced by the process of droplet formation in a T-junction microdroplet generator,” Sens. Actuators Phys., vol. 272, pp. 11–17, Apr. 2018, doi: 10.1016/j.sna.2018.01.013.

[58] X. Wang, A. Riaud, K. Wang, and G. Luo, “Pressure drop-based determination of dynamic interfacial tension of droplet generation process in T-junction microchannel,” Microfluid. Nanofluidics, vol. 18, no. 3, pp. 503–512, Mar. 2015, doi: 10.1007/s10404-014-1449-0.

[59] P. Garstecki, M. J. Fuerstman, H. A. Stone, and G. M. Whitesides, “Formation of droplets and bubbles in a microfluidic T-junction—scaling and mechanism of break-up,” Lab. Chip, vol. 6, no. 3, p. 437, 2006, doi: 10.1039/b510841a.

[60] “Microseal BIO RAD,” Microseal “B” PCR Plate Sealing Film, adhesive, optical #MSB1001. https://www.bio-rad.com/en-ca/sku/msb1001-microseal-b-pcr-plate-sealing-film-adhesive-optical?ID=MSB1001.

[61] T.-K. Chiu, K.-F. Lei, C.-H. Hsieh, H.-B. Hsiao, H.-M. Wang, and M.-H. Wu, “Development of a Microfluidic-Based Optical Sensing Device for Label-Free Detection of Circulating Tumor Cells (CTCs) Through Their Lactic Acid Metabolism,” Sensors, vol. 15, no. 3, pp. 6789–6806, Mar. 2015, doi: 10.3390/s150306789.

[62] T. Dong and C. Barbosa, “Capacitance Variation Induced by Microfluidic Two-Phase Flow across Insulated Interdigital Electrodes in Lab-On-Chip Devices,” Sensors, vol. 15, no. 2, pp. 2694–2708, Jan. 2015, doi: 10.3390/s150202694.

[63] Z. Wang, “Detection and Automation Technologies for the Mass Production of Droplet Biomicrofluidics,” IEEE Rev. Biomed. Eng., vol. 11, pp. 260–274, 2018, doi: 10.1109/RBME.2018.2826984.

[64] S. Aristilde, G. Rodrigues, F. Fruett, and C. M. B. Cordeiro, “Optofluidic Device based on a 3D Printed Chip and a Sensing Tilted Fiber Bragg Gratings,” in 2018 SBFoton International Optics and Photonics Conference (SBFoton IOPC), Campinas, Oct. 2018, pp. 1–4, doi: 10.1109/SBFoton-IOPC.2018.8610934.

[65] J. Wu, L. Pei, X. He, Y. Cui, S. Xuan, and X. Gong, “Study on nonlinear magnetic droplets in a flow-focusing generator,” Appl. Phys. Lett., vol. 115, no. 3, p. 031903, Jul. 2019, doi: 10.1063/1.5104296.

[66] X. Hu, X. Lin, Q. He, and H. Chen, “Electrochemical detection of droplet contents in polystyrene microfluidic chip with integrated micro film electrodes,” J. Electroanal. Chem., vol. 726, pp. 7–14, Jul. 2014, doi: 10.1016/j.jelechem.2014.05.005.

[67] X. Lin et al., “A microfluidic chip capable of switching W/O droplets to vertical laminar flow for electrochemical detection of droplet contents,” Anal. Chim. Acta, vol. 828, pp. 70–79, May 2014, doi: 10.1016/j.aca.2014.04.023.

[68] P. K. Isgor, M. Marcali, M. Keser, and C. Elbuken, “Microfluidic droplet content detection using integrated capacitive sensors,” Sens. Actuators B Chem., vol. 210, pp. 669–675, Apr. 2015, doi: 10.1016/j.snb.2015.01.018.

[69] M. Demori, V. Ferrari, P. Poesio, and D. Strazza, “A microfluidic capacitance sensor for fluid discrimination and characterization,” Sens. Actuators Phys., vol. 172, no. 1, pp. 212–219, Dec. 2011, doi: 10.1016/j.sna.2011.07.013.

[70] L. C. Duarte, C. L. S. Chagas, L. E. B. Ribeiro, and W. K. T. Coltro, “3D printing of microfluidic devices with embedded sensing electrodes for generating and measuring the size of microdroplets based on contactless conductivity detection,” Sens. Actuators B Chem., vol. 251, pp. 427–432, Nov. 2017, doi: 10.1016/j.snb.2017.05.011.

[71] C. Elbuken, T. Glawdel, D. Chan, and C. L. Ren, “Detection of microdroplet size and speed using capacitive sensors,” Sens. Actuators Phys., vol. 171, no. 2, pp. 55–62, Nov. 2011, doi: 10.1016/j.sna.2011.07.007.

[72] X. Han, Z. Su, Y. Xu, and Q. Liu, “Microdroplet event recognition and volume detection system based on flexible printed circuit electrode,” J. Phys. Conf. Ser., vol. 1520, p. 012004, Apr. 2020, doi: 10.1088/1742-6596/1520/1/012004.

[73] G. Nagesh, H. Wang, D. S.-K. Ting, and M. J. Ahamed, “Development of a rapid manufacturable microdroplet generator with pneumatic control,” Microsyst. Technol., Oct. 2020, doi: 10.1007/s00542-020-05052-9.

[74] W. Wei, F. Wu, S. Guo, J. Guo, Y. Ji, and X. Ma, “Numerical simulation of influence parameters during droplet generation in a microfluidic T-junction,” in 2014 IEEE

International Conference on Mechatronics and Automation, Tianjin, China, Aug. 2014, pp. 66–71, doi: 10.1109/ICMA.2014.6885673.

[75] C.-L. Azzopardi, F. Chollet, N. Tarchichi, and J.-F. Manceau, “Integration of electrodes with diphasic microfluidics for capacitance tuning,” in 2017 Symposium on Design, Test, Integration and Packaging of MEMS/MOEMS (DTIP), Bordeaux, France, May 2017, pp. 1–4, doi: 10.1109/DTIP.2017.7984466.

VITA AUCTORIS

NAME: Gnanesh Nagesh

PLACE OF BIRTH: Mysore, India

YEAR OF BIRTH: 1994

EDUCATION: ATME college of engineering, B.E, Mysore, IN, 2016

University of Windsor, MASc, Windsor ON, 2021

PUBLICATIONS: **Conference papers, poster, and journal paper**

1. G. Nagesh, H. Wang, D. S.-K. Ting, and M. J. Ahamed, "Development of a rapid manufacturable microdroplet generator with pneumatic control," Microsyst. Technol., Oct. 2020, https://doi: 10.1007/s00542-020-05052-9.
2. G. Nagesh, D. S.-K. Ting, and M. J. Ahamed, "Capacitive detection and characterizing of droplets in a T-junction-based droplet generator". (Under-revision)
3. Gnanesh Nagesh, David S-K Ting, Mohammed Jalal Ahamed, "Modeling and Experimental Analysis of Pneumatically Controllable T-Junction-Based Droplet Generation", Technical presentation (Abstract only), ASME 2021, IMECE.